Lithos 177 (2013) 470–491

Contents lists available at ScienceDirect

Lithos

journal homepage: www.elsevier.com/locate/lithos

Petrogenesis of migmatites and leucogranites from Sierra de Molinos, Salta, Northwest Argentina: A petrologic and geochemical study

Alfonso M. Sola [a,b,*], Raúl A. Becchio [a,b], Márcio M. Pimentel [c]

[a] Universidad Nacional de Salta, Salta Capital, Argentina
[b] Consejo Nacional de Investigaciones Científicas y Técnicas (CONICET), Argentina
[c] Universidade de Brasília, Instituto de Geociências, Brazil

ARTICLE INFO

Article history:
Received 2 April 2013
Accepted 24 July 2013
Available online 2 August 2013

Keywords:
Migmatites
Leucogranites
Geochemistry
Partial melting
NW Argentina
Famatinian Belt

ABSTRACT

In Sierra de Molinos, Eastern Cordillera, NW Argentina the relationship between different components of an anatectic system developed in high temperature and low pressure conditions (<800 °C and 4–6 kbar) can be observed. This allows the direct insight on the origin of migmatites and granites by anatexis of psammo–pelitic metasedimentary rocks. Four principal rock types have been recognized in Sierra de Molinos 1) metasedimentary rocks, assigned to the Puncoviscana Formation, 2) metatexite migmatites, 3) diatexite migmatites and 4) anatectic granitoids including: leucogranites, trondhjemites and pegmatite/aplitic dykes. The metamorphic grade increases from phyllites and schists at sub-greenschist and greenschist facies in the west, to upper amphibolite facies migmatites in the east. The mineral assemblages indicate a progressive increase in temperature without a significant change in pressure. The ages obtained for granitoids and migmatites are identical within analytical errors and indicate that the metamorphic peak and anatectic granite generation occurred at ca. 470 Ma.

We use petrological and geochemical variations to investigate the formation of granite magma from migmatites that derived from metasedimentary protoliths. This provides evidence of the processes that occur during the evolution (melting, segregation and crystallization stages) of partially molten terranes, for which particular components: protolith, residuum and melt fractions are identified. Mass balance calculations are used to estimate the degree of partial melting and the degree of melt extraction in migmatites. Petrological and compositional data suggest that migmatites from this region are the result of open system processes and that fluid-absent melting played a major role in the formation of migmatites and leucogranites. The geochemical evidence suggests that the compositional variation within the anatectic rocks from Molinos can be understood as a result of 1) variable degrees of melt–residuum separation and 2) fractional crystallization of the anatectic melt. Compared to the protolith, most of the migmatites have melt-depleted compositions (up to 0.25 of melt extraction). In the same fashion most of the leucosomes represent cumulate products of fractional crystallization. This means that they have lost some liquid of evolved composition and represent evidence of the melt extraction pathways and linkage to the magma ascent conduits.

1. Introduction

Partial melt of the crust can give rise to granite bodies that range in scale from centimeter-sized leucosome in migmatites, to large intrusive plutons, and felsic volcanic sequences exposed in an area of several thousands of km^2. Anatexis may occur in a number of different ways that largely depends on the interplay of source mineralogy, pressure–temperature conditions and fluid regime during high temperature metamorphism (e.g. Clemens and Droop, 1998; Stevens and Clemens, 1993). Migmatite terranes constitute, therefore, excellent places to study the link between high grade metamorphism, the partial melting process and the origin of diverse scale granitic bodies (e.g. Brown, 2001). Highly evolved peraluminous leucogranites usually display chemical and isotopic heterogeneities even within single plutons that may be attributed several processes that in most instances, are open to discussion. Since psammo–pelitic migmatite zones are potential sources for peraluminous leucogranites, a comparison between leucosomes and leucogranites may help to understand the origin of many of such chemical variations. In Sierra de Molinos, Eastern Cordillera, NW Argentina (Fig. 1) the different components of an anatectic system that is developed in high temperature and low pressure conditions (HT/LP) are exposed, which allows the direct observation on the origin of migmatites and granites by anatexis of psammo–pelitic metasedimentary rocks. Although the occurrence of migmatites and anatectic rocks has been widely described in this section of the Famatinian belt, the study of partial melting remains qualitative and the degree of partial melting has not been estimated quantitatively (e.g. Büttner et al., 2005; Lucassen et al., 2011). We use petrological and geochemical variations to investigate the formation of granite magma

* Corresponding author at: Universidad Nacional de Salta, Avda. Bolivia 5150, Zip Code: 4400, Argentina. Tel.: +54 387 4255441.
E-mail address: alfonsoseptimo@yahoo.com.ar (A.M. Sola).

0024-4937/$ – see front matter © 2013 Elsevier B.V. All rights reserved.
http://dx.doi.org/10.1016/j.lithos.2013.07.025

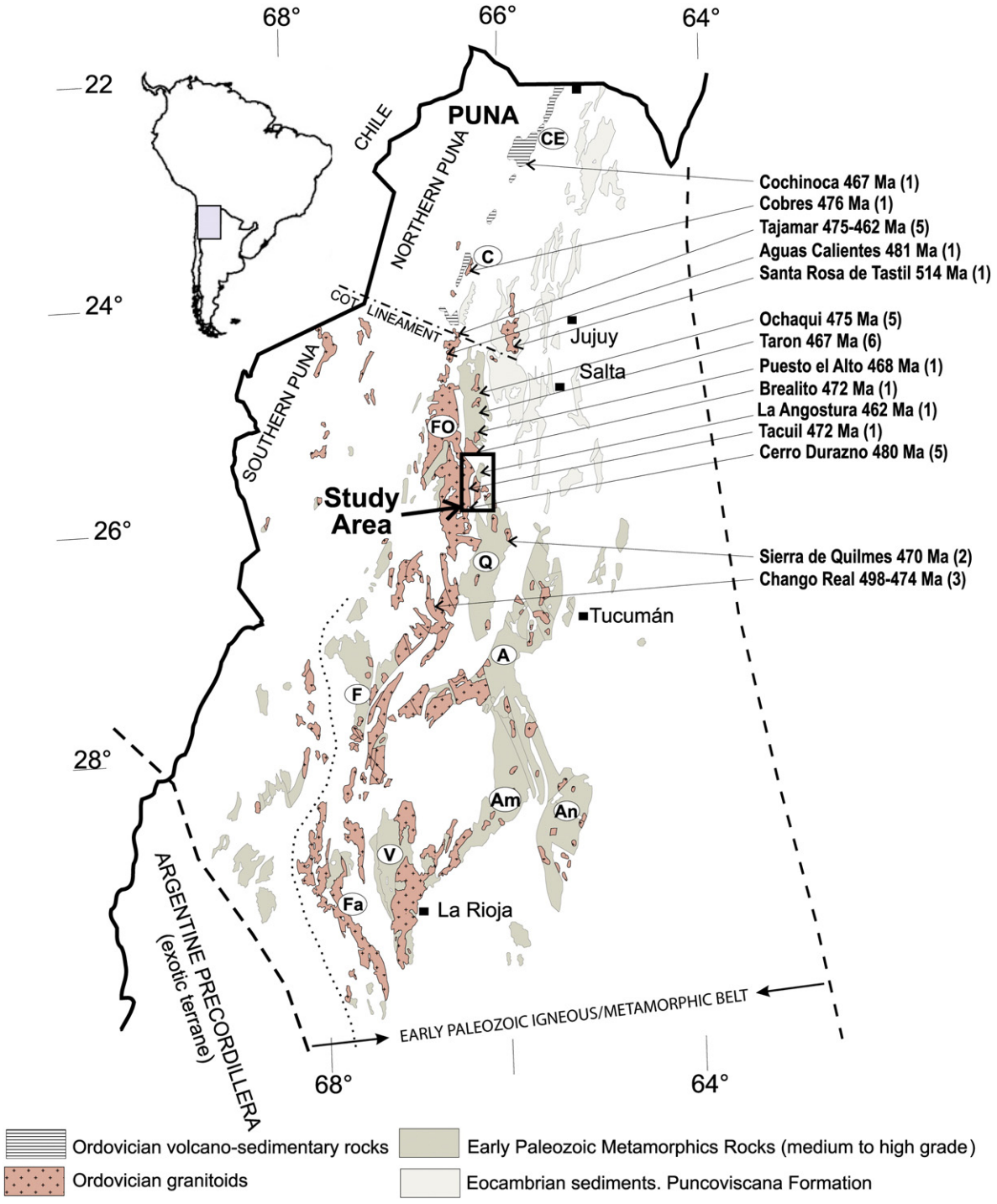

Fig. 1. Geological map showing the distribution of Paleozoic magmatic and metamorphic rocks, Puncoviscana Formation, the principal Paleozoic Mountain Ranges and the Early Paleozoic Mobile Belt. The crystallization ages of Early Paleozoic granitoids are from: (1) U–Pb monazite (Lork and Bahlburg, 1993; Lork et al., 1989), (2) U–Pb monazite and titanite (Büttner et al., 2005), (3) Rb–Sr whole-rock (García and Rossello, 1984), (4) U–Pb zircon (Haschke et al., 2005), (5) U–Pb zircon (Viramonte et al., 2007), (6) U–Pb zircon (Dominguez et al., 2006). Principal Paleozoic Mountain Ranges A = Aconquija, Q = Quilmes, Am = Ambato, F = Fiambala, An = Ancasti, V. Velasco, Fa = Famatina, FO = Filo de Oire Grande, CE = Cochinoca Escaya. C = Cobres.

from migmatites and provide evidence of the processes that occur during melting, segregation and crystallization stages. Mass balance calculations are used to estimate the degree of partial melting and the degree of melt extraction in migmatites. Additionally, U–Pb zircon and Sr–Nd whole-rock isotopic data are reported for different rock types to further examine the connection between these units.

The aim of our study is to describe and evaluate the association between lower grade Puncoviscana metasedimentary rocks, migmatites and leucogranites from a multidisciplinary perspective by means of field, petrographic, geochemical, geochronological (U–Pb) and Sr–Nd isotopic data. Our results have implications to other areas along the Puna–Eastern Cordillera boundary and towards the Northern Sierras

Pampeanas, where the anatectic processes related with the genesis of the low volume (leuco) granitic magmas are observed.

2. Geological setting

The study area is located in the Calchaquí Valleys at the transition between the geologic provinces of Eastern Cordillera and the Northern Sierras Pampeanas, northwestern Argentina (Fig. 1). The sedimentary protolith of the metamorphic rocks consists of a turbiditic sequence assigned to the Puncoviscana Formation (Neoproterozoic to Early Cambrian). This sequence consists mainly of turbidites (Aceñolaza et al., 1988; Jêzek, 1990; Omarini et al., 1999) deposited in a large sedimentary basin extending in the N–S direction from Bolivia to central Argentina (~33°S) roughly between 64° and 68°W (Rapela et al., 1990). A recent U–Pb detrital zircon analysis from classic sequences of this unit confirmed a maximum depositional age of late Early Cambrian based on the younger zircon population of approximately 523–534 Ma (Adams et al., 2008). The turbiditic greywackes and pelites of the Puncoviscana Formation were tightly folded and affected by low grade metamorphism during the Pampean Orogeny in the Early to Middle Cambrian (Aceñolaza et al., 2000). During the Famatinian Orogeny (~490 to 435 Ma), these rocks were metamorphosed into phyllites, schists, gneisses, culminating in anatectic migmatites and associated plutonism (Becchio et al., 1999; Büttner et al., 2005; Lucassen et al., 2000; Rossi et al., 1992). Thus, the western margin of Gondwana seems to be affected by successive events of medium to high grade metamorphism during the Early Paleozoic (Lucassen and Becchio, 2003). Deformation appears to have been accomplished chiefly along ductile deformation zones during the Ordovician (Hongn and Mon, 1999; Hongn et al., 1996). Emplacement of the granitoid plutons occurred largely between 480 and 460 Ma (see Fig. 1) being coeval with high grade metamorphism and apparently associated with N–S deformation zones and NW–SE shear zones (Hongn et al., 1996; Hongn and Becchio, 1999; Hongn and Mon, 1999). However, the precise age relationships between magmatism and metamorphism/deformation are not well known (Hongn et al., 1996; Hongn and Becchio, 1999). Recently, Wegmann et al. (2008) suggested that ductile deformation could have been active during magmatism and persists afterwards under greenschist facies P–T conditions, reporting Rb–Sr mineral (white mica and K-feldspar) isochron ages of 437 ±4 Ma and 428 ± 5 Ma for mylonitic rocks in a shear zone, located approximately 25 km south of the study area (Agua Rosada Shear Zone).

Migmatites yielded the U–Pb monazite age of ca. 467 Ma (Lork and Bahlburg, 1993), northward of the study area, and of ca. 470 Ma (U–Pb monazite age) in the Sierras de Quilmes, coinciding with ages of granitic plutonism (Büttner et al., 2005).

Several geodynamic models have been proposed to explain the tectonic significance of Late Proterozoic–Paleozoic metamorphic complexes at the western margin of Gondwana. Two contrasting models with internal variations have been suggested: (i) amalgamation of an allochthonous terrane either in the Neoproterozoic or in the Early Paleozoic (Bahlburg and Hervé, 1997; Ramos, 1999, 2008) and (ii) development of an intra-cratonic igneous/metamorphic belt with a long lasting high-thermal gradient during both the Pampean and Famatinian orogenies (Aceñolaza et al., 2000; Büttner et al., 2005; Lucassen et al., 2000, 2011). The high-thermal gradient is represented regionally by the widespread occurrences of granites and high temperature/low pressure (HT–LP) metamorphic rocks along an N–S belt extending from the Eastern Cordillera through the Sierras Pampeanas (Fig. 1). The ages of extensive anatexis spread roughly between 500 and 440 Ma (references above). As a consequence, a considerable part of the Puncoviscana Formation reached upper amphibolite and granulite facies conditions (e.g. Sierras de Quilmes) and partial melting started in the medium to high level of the crust. Numerous leucogranite plutons and pegmatite swarms formed along this high temperature axis.

2.1. The granites from the Famatinian Belt

Pankhurst et al. (2000) recognized three granitoid types within the Famatinian Belt: a) a tonalite–trondhjemite–granodiorite (TTG) group b) S-type granites and c) a metaluminous I-type gabbro-monzogranite suite. All three distinct types were essentially contemporaneous within the Tremadoc–Llanvirn interval. Particularly the TTG and the S-type granites represent the northern extension of the Famatinian belt. The TTG group occurs as small to medium-sized peraluminous plutons composed essentially of quartz, plagioclase, muscovite, minor K-feldspar and biotite, apatite, zircon, titanite and rare occurrences of epidote. Examples were first described in the Sierra de Cachi, in the northern Sierras Pampeanas by Galliski and Miller (1989), and dated as Early Ordovician by Lork et al. (1991). The S-type group forms prominent cordierite, sillimanite and two mica-bearing batoliths constituting the so-called “Faja Eruptiva de la Puna Oriental”, which has been the subject of a large number of studies aimed at understanding its origin, evolution and tectonic significance (e.g. Fernandez et al., 2008; Toselli et al., 2002; Viramonte et al., 2007). Although S-type granites and trondhjemites display similar ages and rare earth element distribution, differences in some major and trace element composition and the lack of isotopic data, raise doubts on the origin of these rocks, especially the TTG. Galliski and Miller (1989), Pankhurst et al. (2000) and Méndez et al. (2006) suggest variable degrees (5–10%) of partial melting of a depleted gabbroid source at 10–12 kbar for trondhjemites. However, most of these rocks lack the typical discriminating features of TTG such as strong depletion of heavy REE and high La/Yb ratios, related to the melting of a mafic source where garnet, clinopyroxene or hornblende are residual phases.

3. Field relationships and petrography of principal rock types

Metamorphism in the Sierra de Molinos is the subject of ongoing research and the preliminary results are briefly presented here. Specifically, the Puncoviscana Formation metasediments show a continuous transition from low and medium metamorphic grade to anatectic migmatites (metatexites and diatexites). The metamorphic grade increases from west to east, from phyllites and schists at sub-greenschist and greenschist facies in the west, to high amphibolite facies migmatites on the eastern side of the range. The mineral assemblages appear to be the result of a progressive increase in temperature without a significant change in pressure. Metamorphism displays typical features of high temperature and low pressure conditions (e.g. Spear et al., 1999; Yardley, 1989): i) no kyanite has been found in the area, but sillimanite is widespread as the metamorphic grade increases, ii) cordierite is very common and occurs from low to intermediate metamorphic grades, iii) garnet is scarce or absent in most metamorphic units and iv) migmatites are developed above the so-called “second sillimanite isograd” with progression from sillimanite–K-feldspar assemblages to cordierite–K-feldspar assemblages in higher grade migmatites. Only rough estimates are possible for the pressure conditions during migmatization due to the lack of assemblages suitable for geobarometry, however, at the present 4 to 6 kbar are probably reasonable values.

Four principal rock types have been recognized in Sierra de Molinos 1) metasedimentary rocks, 2) metatexite migmatites, 3) diatexite migmatites and 4) anatectic granitoids which include leucogranites, trondhjemites and pegmatite/aplitic dykes. Following this subdivision we describe the different rock types and how they are related.

3.1. Metasedimentary rocks

This group encompasses the non-migmatitic metasedimentary rocks. The lowest grade metasediments crop out in the northeastern part of the area and are assigned to the Puncoviscana Formation (Fig. 2). This sequence of turbiditic metasedimentary rocks consists predominantly of centimeter to decimeter scale layers of contrasting

composition inferred to be bedding. The layering consists of alternating chlorite-clay-rich pelitic layers, and quartzo-feldspar-rich psammitic layers with subordinate calc-silicate rocks. Some pelitic layers contain gray (<2 mm diameter) poikiloblasts, which represent cordierite later altered to fine grained micas. The sequence exhibits tight isoclinal folding with axial plane cleavage well developed in pelitic layers and multistage brittle deformation features. Under the microscope pelitic and psammitic domains are identified. Pelitic domains consist essentially of chlorite, white mica, quartz plus rutile, zircon, monazite and opaque as accessory minerals. Psammitic domains are composed of quartz, feldspar, minor chlorite and accessory rutile, monazite, zircon and opaque minerals.

Before the appearance of the first leucosomes, the mineral assemblage of metapelitic layers consists essentially of muscovite, biotite, quartz, cordierite and plagioclase, with accessory amounts of tourmaline, apatite, zircon and opaque minerals (Fe–Ti oxides).

3.2. Metatexite migmatites

The onset of partial melting and the former occurrence of leucosome veins within metapelitic layers is marked by the disappearance of the primary muscovite and the appearance of widespread sillimanite and K-feldspar in the mineral assemblage. Based upon the melt fraction retained, migmatitic rocks are subdivided into metatexites

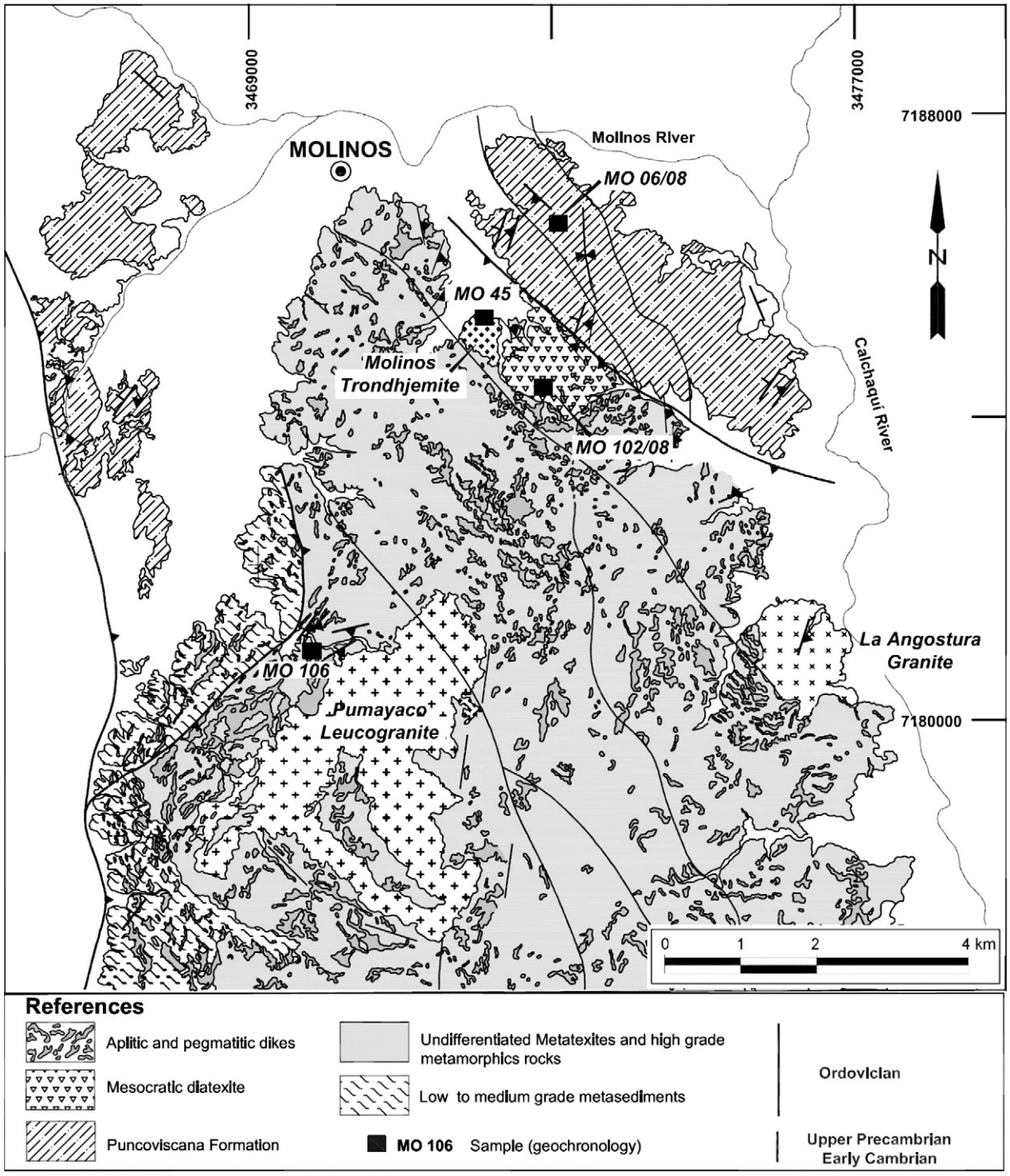

Fig. 2. Geologic map from Sierra de Molinos Igneous–metamorphic complex and sample locations for U–Pb dating.

and diatexites. Metatexite is defined as a migmatite that preserves evident pre-partial melting structures such as layering, foliation or bedding and where the fraction of melt was low (Brown, 1973; Sawyer, 2008). The Molinos metatexite migmatites are mainly stromatic consisting on numerous thin (commonly 2 mm to 2 cm) and laterally persistent bands of light colored quartzo-feldspatic leucosomes usually bounded by dark biotite-rich melanosomes (e.g. Fig. 3a). Stromatic metatexites constitute the most abundant morphologic variety among migmatites in the study area. Most leucosomes are laterally continuous and parallel to the main foliation and compositional layering but some are located at dilatant sites such as interboudin partitions and small shear bands outlining net-like patterns and cross-cutting the main foliation (Fig. 3c). The leucosomes located at such dilatant sites are commonly coarser grained than leucosomes parallel to the foliation. Leucosomes

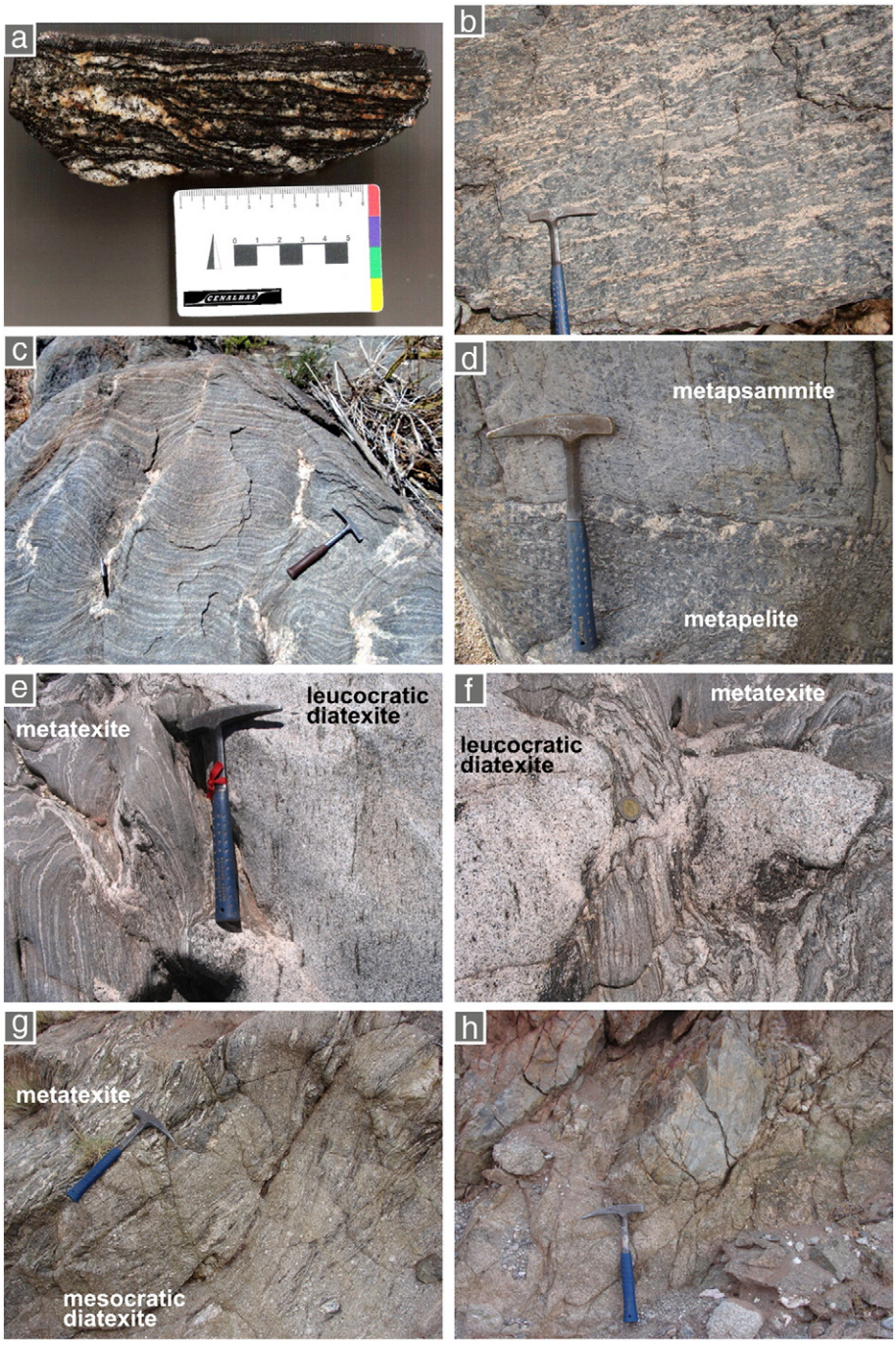

Fig. 3. Photographs illustrating field occurrence and genetic relations of Sierra de Molinos migmatites. a) Polished slice of a Sil–Kfs metatexite migmatite showing the stromatic structure defined by numerous thin and laterally persistent bands of leucosomes usually bounded by dark biotite-rich melanosomes. b) Stromatic structure in a cordierite-rich metatexite, Note the abundance of peritectic cordierite in some of the layers. Many layers are interpreted as former leucosomes that have lost melt. c) Leucosomes injected into low pressure sites in boudinaged stromatic migmatites. d) Bedded structure in a metatexite. The neosome, composed by cordierite and some leucosome patches, is confined to metapelitic layers (bottom). e) Detail on the contact between a folded stromatic migmatite (left) and a leucocratic diatexite (right). Note the alignments of mafic schlieren following the contact and defining a syn-anatectic flow structure. f) Part of the leucocratic diatexite intruding into the host composed by stromatic migmatites. g) Transition from a metatexite migmatite (top left) to the mesocratic diatexite (right side). h) Detail on a metapsammitic resister (top center) into the mesocratic diatexite. In this photograph the aspect of the mesocratic diatexites is homogeneous.

may be alternatively distributed as irregular patches or lenses. Many of these field relationships are shown in Fig. 3.

According to their mineral assemblages, metatexites were subdivided into two main groups; the first one containing sillimanite and K-feldspar in the neosome (Sil–Kfs metatexites) and the second group dominated by cordierite and K-feldspar where sillimanite is scarce or absent (Crd–Kfs metatexites). Leucosomes in the Sil–Kfs metatexites are mainly trondhjemitic being composed of quartz, plagioclase, muscovite, tourmaline and rare biotite with accessory sillimanite or cordierite. The melanocratic host matrix in the Sil–Kfs metatexites exhibits lepidoblastic schistose texture and mineral assemblage composed of biotite, quartz, fibrolitic sillimanite, K-feldspar (microcline/microperthite), plagioclase and retrograde, possibly late magmatic, muscovite with accessory apatite, tourmaline, zircon and monazite. The main foliation is defined by preferred orientation of biotite and sillimanite.

In the Crd–Kfs metatexites, the leucosomes contain quartz, K-feldspar, plagioclase, cordierite, subordinate biotite and apatite. The mesosome and melanosome show grano-lepidoblastic texture consisting of biotite, K-feldspar, cordierite, plagioclase and quartz. The main foliation is defined by the preferred orientation of biotite. Sillimanite is absent in most samples and its rare occurrence restricts to minor amounts inside or surrounded by cordierite. Cordierite and K-feldspar are abundant (cordierite may achieve 30 vol.%) in most metapelitic layers occurring as porphyroblasts of up to 7 cm in size, enclosing small round-shaped inclusions of biotite, quartz and occasionally sillimanite and tourmaline. Cordierite and K-feldspar porphyroblasts usually develop inclusion-free rims when they are adjacent to leucosomes, whereas inside the melanosome/mesosome they have inclusion-rich areas; these features suggest crystallization from a melt or growth in a melt-rich environment. Apatite, tourmaline, zircon and monazite are the common accessory phases. Zircon and monazite frequently form inclusions in major minerals such as biotite and cordierite.

Some of the metatexite migmatites are locally too depleted in leucosome and enriched in mafic mineral suggesting melt loss (Fig. 3b, d).

3.3. Diatexite migmatites

Diatexites represent migmatites with a large melt fraction where pre-partial melting structures are normally replaced by syn-anatectic-flow structures (Brown, 1973; Sawyer, 2008). Diatexites in Molinos show a considerable range in morphologies. Two main types can be recognized based on textural and mineralogical aspects: leucocratic diatexites and mesocratic diatexites.

3.3.1. Leucocratic diatexites

Leucocratic diatexites occur as meter scale bodies showing intrusive relationships within the metatexites (Fig. 3e–f). Locally these bodies may connect with microplutons and granitic dykes. Fragments of stromatic metatexites with internal layering may be present inside these leucocratic bodies. These diatexites are gray, equigranular, fine grained rocks consisting of plagioclase, quartz, biotite (<15%), muscovite, sillimanite, apatite and tourmaline. The K-feldspar is rare or absent. Biotite is normally distributed uniformly but may locally form biotite- or biotite–sillimanite-rich *schlieren* that outlines a flow-banding or layering in the rock. Sillimanite is texturally prismatic and less abundant than in metatexites. Quartz grains are not greatly strained and igneous textures are preserved overall (Fig. 4e). The apatite occurs abundantly as irregular shaped crystals that may locally form aggregates.

3.3.2. Mesocratic diatexites

Mesocratic diatexites display granoblastic textures consisting of quartz, biotite, K-feldspar, plagioclase, cordierite, muscovite, with accessory sillimanite, tourmaline and apatite. These diatexites display greater contents of mafic minerals. Biotite does not show a strong preferred orientation and it is generally retrograded to chlorite. Cordierite forms anhedral to subhedral grains which seem to be completely replaced by fine grained retrograde aggregates (Fig. 4f). The K-feldspar (microcline) commonly contains numerous round-shaped inclusions of biotite and quartz. Most of the muscovite is assumed to be late and occurs as large flakes replacing sillimanite and biotite or forming symplectite with quartz. Plagioclase and quartz preserve locally polygonal shapes.

The mesocratic diatexite contains scattered small schollen. Most of the schollen are small fragments of biotite–cordierite–sillimanite–rich melanosome and are probably the remnants of larger rafts derived from stromatic metatexite (Fig. 3g). Other rafts consist of resister lithologies such as psammitic blocks and disrupted quartz veins (Fig. 3h).

3.4. Leucogranites, trondhjemites and pegmatite/aplitic dykes

Granites occur as sheet-like or elliptical-shaped bodies intruding the high grade rocks. There are three main plutons (Fig. 2): the Pumayaco leucogranite (Sola et al., 2010), La Angostura granodiorite and the Molinos trondhjemite.

The granite intrusions consist mostly of fine and medium grained granodiorites to syenogranites containing less than 15% of biotite. Garnet, cordierite, sillimanite and tourmaline are some of the accessory minerals that distinguish the Molinos granites from other granites in the region (Fig. 4g). Garnet form 0.5–3 mm sized zoned euhedral crystals quite similar to that found in aplitic and pegmatitic dykes. Cordierite is anhedral, extremely altered (pinnitized) and inclusion-free. Basically two assemblages are recognized: muscovite–biotite leucogranites and garnet–tourmaline leucogranites.

Trondhjemites occur as small elongated sheet-like or elliptical plutons widespread along the range. The trondhjemites are composed of a simple assemblage of plagioclase, quartz and biotite. K-feldspar is typically absent or rare as an interstitial phase. Tourmaline is commonly present.

Pegmatites and aplites intrude as near-vertical dyke swarms into the high grade metamorphic rocks (Fig. 2). The pegmatites consist of quartz, microcline, plagioclase, muscovite ± tourmaline ± garnet. The aplites are composed chiefly of quartz, microcline, plagioclase, tourmaline, muscovite and garnet and may exhibit diffuse banding defined by alternation of black tourmaline and garnet-rich layers with fine grained quartz–feldspar-rich layers. At least three types of pegmatitic dykes occur in the Sierra de Molinos. The first type, assumed to be the oldest, is isoclinally folded within the metamorphic host rocks and occurs as disrupted dykes cut by the granites. The second type intruded parallel to the foliation and to the migmatitic layering and is commonly boudinaged. The third group is formed by dykes cross-cutting the migmatitic layering, which suggests intrusion after migmatization. The field relationships reveal several intrusion episodes indicating that most of the pegmatites may not be directly related to granites. Furthermore, the pervasive occurrence of pegmatites suggests that the major source of pegmatite liquids is located somewhere deeper in the crust.

4. Geochemistry

Major and trace element contents were determined by X-ray fluorescence (XRF) and Inductively Coupled Plasma Mass Spectrometry (ICP-MS) for representative samples of: pelite (n = 3) and psammite (n = 3) layers from Puncoviscana metasedimentary rocks; metatexite migmatites (n = 11); leucosomes (n = 6) and melanosomes (n = 5) from metatexite migmatites; leucocratic diatexites (n = 2); mesocratic diatexites (n = 4); leucogranite (n = 16); trondhjemites (n = 2) (Molinos Trondhjemite) and garnet-bearing pegmatite (n = 1). Representative analyses are given in Table 1. Details on the analytical procedures are given in Appendix A.

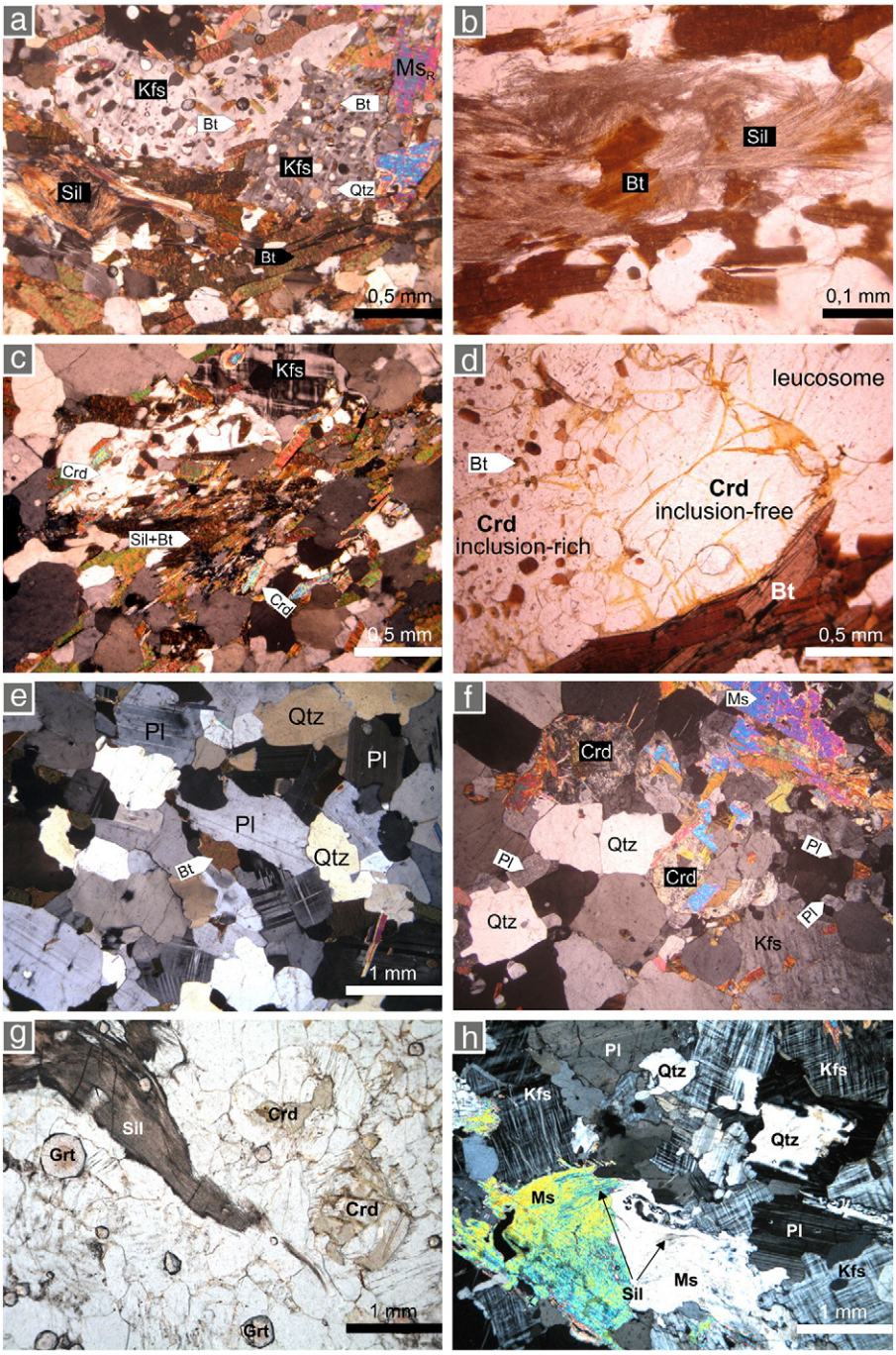

Fig. 4. Photomicrographs of rocks in Sierra de Molinos. a) Melanocratic matrix in a Sil–Kfs metatexite migmatite. The K-feldspar porphyroblasts contain numerous inclusions of quartz and biotite. The foliation is defined by the preferred orientation of biotite and sillimanite wrapping around the K-feldspar porphyroblasts. b) Detail of the intergrowth of sillimanite (fibrolite) and biotite defining the main foliation in a Sil–Kfs metatexite. c) Cordierite replacing sillimanite + biotite in a Crd–Kfs metatexite. d) Cordierite porphyroblast adjacent to a leucosome with inclusion-free rim and inclusion-rich core. These features suggest crystallization from a liquid or growth in a melt-rich environment. e) Igneous texture in a leucocratic diatexite migmatite. This rock is composed largely by subhedral to euhedral crystals of plagioclase forming a framework of touching crystals. The interstices of the feldespar framework are filled with quartz. f) Mesocratic diatexite migmatite. The cordierite forms subhedral grains completely replaced by fine grained aggregates. Plagioclase and quartz may locally preserve polygonal shapes. The retrograde muscovite is very common. g) Leucogranite sample with accessory sillimanite (fibrolite), cordierite and garnet. h) Leucogranite sample of syenogranitic composition.

4.1. Metasedimentary rocks

Field observations suggest that metasedimentary rocks of Puncoviscana Formation are the likely protolith of migmatites and anatectic granitoids in Sierra de Molinos (e.g. Fig. 3). For this reason the geochemical features of these metasediments (metapelites and metapsammites) are described first. Metapelites dominate the Puncoviscana sequence (samples: MO104/08, MO40 and MO25). They show SiO_2 contents ranging from ~60 to ~66 wt.% (Table 1). They are rich in FeO_t, MgO, and TiO_2 with a composition close to ordinary pelites, with $K_2O > Na_2O$ and low CaO (Taylor and McLennan, 1985). Their trace element contents and the rare earth elements (REE), with their characteristic fractionated pattern and pronounced negative Eu anomaly are well within the compositional range of post-archean pelites (Taylor and McLennan, 1985). Psammites are the less abundant metasediments (samples: MO103/08, MO24 and MO49). With respect to metapelites,

Table 1
Major (wt.%) and trace element (ppm) composition of metasedimentary rocks, migmatites (whole-rock and component compositions) and granitoids from Sierra de Molinos. LOI: Loss on ignition; n/d: below limit of detection. *Total Fe as Fe_2O_3.

Rock	Metatexite (Sil–Kfs)								Melanosome					Leucosome			
Sample	MO39	MO26	MO44	MO31	MO37	MO38	MO105/08	MO108/08	Melgral	Mel-1	Mel-2	Mel-3	Mel-4	MO53	MO106/08	Leu-1	Leu-2
SiO2	69.45	65.30	66.55	65.48	62.45	64.57	64.53	66.34	64.28	63.40	61.74	63.66	63.20	69.28	72.85	74.50	74.40
TiO2	0.60	0.71	0.62	0.68	0.79	0.69	0.68	0.63	0.69	0.82	0.74	0.73	0.86	0.34	0.16	0.07	0.12
Al2O3	14.22	16.51	15.97	15.98	16.85	16.56	16.62	15.41	16.76	15.80	16.59	16.23	15.80	16.12	14.69	14.30	14.25
Fe2O3*	4.84	6.21	5.34	5.99	7.24	6.78	6.07	5.51	6.34	6.66	6.89	6.28	6.70	2.83	1.32	0.77	1.19
MnO	0.10	0.10	0.09	0.10	0.12	0.12	0.11	0.11	0.11	0.12	0.12	0.11	0.11	0.06	0.03	0.02	0.03
MgO	2.03	2.56	2.33	2.62	3.13	2.98	2.67	2.43	2.70	2.72	3.42	2.85	2.77	1.23	0.62	0.27	0.44
CaO	1.77	1.35	1.07	0.88	0.73	0.76	0.98	1.46	1.19	1.34	1.40	1.11	1.13	2.97	0.88	2.11	2.84
Na2O	2.50	2.89	1.96	2.12	1.73	1.79	1.82	2.20	2.52	2.13	2.21	2.20	1.98	4.11	2.09	3.79	4.26
K2O	3.17	3.27	4.33	4.19	4.61	4.54	4.20	3.93	3.65	3.54	4.11	4.41	3.85	1.87	5.44	1.32	0.91
P2O5	0.20	0.18	0.19	0.18	0.14	0.17	0.19	0.21	0.21	0.18	0.16	0.18	0.15	0.31	0.24	0.22	0.30
LOI	0.92	0.90	1.95	0.86	2.61	0.83	1.34	1.05	0.95	1.97	1.75	1.64	1.86	0.70	1.05	1.29	0.89
total	99.80	99.98	100.39	99.08	100.39	99.79	99.20	99.28	99.399	98.7	99.138	99.413	98.5	99.81	99.37	98.8	99.7
Ba	386	306	456	385	417	427	361	470	313	358	397	335	383	138	932	600	306
Rb	148	132	148	143	213.1	187.2	186.7	192	208	212	216	207	199	87.2	118.6	39.4	33.9
Sr	67	127	113	100	80.9	87.1	89.1	112.2	86.8	91.3	83.2	87.4	86.2	210.2	166.9	173.5	183.5
Zr	173	197	160	179	214.2	173.5	200.4	255.4	212	209	241	235	239	154.3	82.9	21	34
Y	37	36	32	35	37.5	32.1	31.1	30.7	34.5	33.8	37.3	35.5	35.5	16.1	16	7.4	13.1
Nb	14	13	13	14	19.1	16.9	16.6	14.8	18	17.5	19.7	19.8	19.2	11.3	5.2	4.1	4
U	3	3	0	0	3.8	3.4	3.7	2.7	3.68	3.43	3.57	5	3.69	1.2	1.8	0.96	1.12
Th	5	0	2	1	18.1	16.4	15.6	14.3	15.9	16.15	17.7	16.65	16.95	4	6	1.09	1.84
Co	73	58	70	69	63.6	70.7	82.3	84.7	48.9	61.4	73.8	62.1	78.4	63.2	134.9	95.9	116.5
V	175	137	121	129	124	109	99	86	106	102	114	108	109	44	11	9	16
La	–	–	–	–	44.1	38.8	41	38.3	42.2	42.2	47.3	45	45.8	18	19.2	4.4	7.1
Ce	–	–	–	–	98.5	80.9	86.5	84.3	86.7	87.1	96.6	91.5	93.8	39.2	40.6	8.8	14.9
Pr	–	–	–	–	11.32	9.79	10.12	9.63	10.45	10.65	11.6	11.1	11.35	4.7	4.71	1.08	1.91
Nd	–	–	–	–	40.5	36.9	39.9	38.3	39.3	38.7	43.4	41.5	42.3	17.5	17.5	4.1	7.5
Sm	–	–	–	–	7.78	6.91	7.7	7.26	8.18	8.36	8.72	8.51	8.52	3.34	3.49	1.06	2.09
Eu	–	–	–	–	1.39	1.31	1.33	1.35	1.41	1.42	1.49	1.42	1.48	1.01	0.83	0.85	1.03
Gd	–	–	–	–	6.68	5.85	6.28	6.18	7.66	7.52	8.15	7.85	7.73	2.98	3.2	1.13	2.14
Tb	–	–	–	–	1.15	1.03	1.02	1.04	1.17	1.15	1.25	1.2	1.19	0.55	0.55	0.23	0.42
Dy	–	–	–	–	6.28	5.69	5.55	5.68	6.76	6.36	7.06	6.81	6.68	3.06	3.01	1.43	2.59
Ho	–	–	–	–	1.29	1.16	1.14	1.14	1.32	1.25	1.4	1.35	1.3	0.57	0.56	0.27	0.51
Er	–	–	–	–	3.56	3.31	3.24	3.32	3.97	3.78	4.18	4.08	3.97	1.64	1.69	0.86	1.38
Tm	–	–	–	–	0.6	0.55	0.53	0.53	0.57	0.54	0.58	0.58	0.56	0.27	0.26	0.12	0.2
Yb	–	–	–	–	3.53	3.17	3.19	3.22	3.82	3.53	3.89	3.77	3.64	1.57	1.44	0.83	1.31
Lu	–	–	–	–	0.55	0.48	0.47	0.47	0.56	0.51	0.57	0.57	0.55	0.23	0.24	0.12	0.18
Hf	–	–	–	–	6.5	5	5.7	6.9	6.2	5.9	6.8	6.6	6.7	4.2	2.3	0.8	1.1
Ta	–	–	–	–	1.3	1.2	1.2	1.2	1.3	1.1	1.3	1.5	1.3	1	0.5	1.2	0.9

(continued on next page)

Table 1 (*continued*)

Rock	Leucosome		Metatexite (Crd–Kfs)			Leucogranite											
Sample	Leu-3	Leu-4	ResMol	ResA	ResB	MO90	MO70	MO76	MO78	MO59	MO34	MO35	MO33	MO55	MO57	MO80	MO82
SiO2	73.82	73.80	61.54	64.90	60.50	74.07	71.64	72.24	76.03	75.06	75.04	75.08	74.86	73.43	71.97	72.72	75.16
TiO2	0.12	0.07	0.70	0.70	0.77	0.01	0.35	0.29	0.05	0.06	0.02	0.16	0.09	0.09	0.27	0.27	0.03
Al2O3	14.64	14.50	16.74	15.60	17.77	15.13	14.59	14.65	14.44	14.50	13.83	13.74	14.36	14.56	14.70	14.77	14.80
Fe2O3*	1.66	0.83	6.59	5.40	7.62	0.42	3.02	2.55	0.64	0.68	0.73	1.76	1.02	0.89	2.46	2.48	0.65
MnO	0.02	0.02	0.12	0.12	0.18	0.20	0.08	0.07	0.02	0.05	0.07	0.07	0.04	0.07	0.08	0.08	0.26
MgO	0.85	0.26	2.98	1.97	3.50	0.21	1.62	1.11	0.18	0.37	0.24	0.71	0.53	0.40	1.06	1.02	0.12
CaO	1.54	3.05	0.91	0.86	0.73	0.20	2.31	2.12	0.52	0.58	0.39	1.05	0.72	0.75	2.05	2.08	0.38
Na2O	2.04	4.82	1.87	2.37	1.98	2.01	3.65	3.95	3.79	4.03	3.74	4.14	3.28	3.80	3.82	4.03	2.75
K2O	2.42	0.75	5.06	4.32	3.70	6.86	2.29	2.44	4.16	4.02	4.30	2.97	4.99	4.18	2.41	2.05	5.87
P2O5	0.34	0.18	0.19	0.19	0.16	0.58	0.18	0.16	0.24	0.24	0.17	0.15	0.23	0.27	0.18	0.20	0.28
LOI	1.75	1.76	1.45	2.08	2.34	0.37	0.49	0.47	0.65	0.52	0.56	0.31	0.57	0.61	0.77	0.59	0.32
Total	99.203	100	98.148	98.6	99.255	100.04	100.205	100.031	100.70	100.10	99.10	100.14	100.68	99.05	99.78	100.29	100.61
Ba	418	180.5	500	529	345	45	181	284	105	56	38	240	212	113	275	235	54
Rb	68.9	25.3	202	191.5	206	289.1	112	128	201	285	157	154	183	352	179	127	163
Sr	84.2	194.5	94.7	115	90.4	20.8	151	163	0	0	4	91	114	26	148	151	0
Zr	83	18	214	158	225	16.9	188	153	20	20	17	68	45	38	142	141	28
Y	12.5	7.8	34.8	28.2	37.7	0.6	29	25	19	18	18	32	25	21	30	29	15
Nb	9.2	3	16.4	17.5	19.7	46.9	9	9	11	11	33	12	9	12	9	10	11
U	2.95	0.89	3	3.49	3.51	4.7	2	n/d	0	1	1	0	1	1	0	0	0
Th	3.95	1.76	16.35	14.15	18.4	0.4	7	4	2	0	2	3	0	1	4	6	0
Co	79.5	178.5	77.7	148.5	122.5	107.8	94	104	89	69	89	86	80	104	76	86	90
V	18	22	105	91	114	44	66	46	5	2	9	32	14	11	47	44	
La	10	6.7	42.9	36.6	47.1	0.6	22.64	35.10	–	–	–	–	–	–	–	–	1.38
Ce	20.8	12.8	88.3	75.9	99.2	0.6	42.46	64.37	–	–	–	–	–	–	–	–	3.35
Pr	2.53	1.54	10.6	9.03	11.6	0.06	5.30	7.65	–	–	–	–	–	–	–	–	0.47
Nd	9.7	5.7	39.2	33.2	43.2	<0.3	20.02	29.19	–	–	–	–	–	–	–	–	1.92
Sm	2.25	1.34	8.1	6.84	8.79	0.1	3.72	5.39	–	–	–	–	–	–	–	–	0.78
Eu	0.77	0.92	1.5	1.44	1.44	0.04	0.71	1.37	–	–	–	–	–	–	–	–	0.01
Gd	2.21	1.35	7.68	6.37	8.16	<0.05	3.29	4.80	–	–	–	–	–	–	–	–	0.70
Tb	0.39	0.25	1.16	0.96	1.27	0.02	0.46	0.65	–	–	–	–	–	–	–	–	0.14
Dy	2.3	1.5	6.71	5.4	7.28	0.12	2.28	3.37	–	–	–	–	–	–	–	–	0.87
Ho	0.46	0.29	1.31	1.08	1.45	<0.02	0.34	0.49	–	–	–	–	–	–	–	–	0.11
Er	1.41	0.84	3.93	3.2	4.33	<0.03	0.82	1.17	–	–	–	–	–	–	–	–	0.32
Tm	0.23	0.12	0.58	0.47	0.62	<0.01	–	–	–	–	–	–	–	–	–	–	0.02
Yb	1.72	0.78	3.71	3.06	3.94	0.06	0.62	0.91	–	–	–	–	–	–	–	–	0.55
Lu	0.27	0.11	0.57	0.47	0.59	0.02	–	–	–	–	–	–	–	–	–	–	–
Hf	3.2	0.6	6.2	4.6	6.4	1.3	–	–	–	–	–	–	–	–	–	–	–
Ta	5.5	1.2	1.1	1.7	1.2	19.2	–	–	–	–	–	–	–	–	–	–	–

Table 1 (*continued*)

Rock	Leucogranite				Leucocratic Diatexite		Pegmatite	Trondhjemite		Metapelite			Metapsammite			Mesocratic diatexite			
Sample	MO56	MO58	MO72	MO77	DtxLeu1	DtxLeu2	MO32	MO46	MO45	MO104/08	MO25	MO40	MO103/08	MO49	MO24	MO61	MO51	MO102/08	MO110/08
SiO2	72.27	75.13	69.58	71.85	68.30	67.00	75.71	69.31	73.89	65.74	59.71	64.79	73.78	71.87	73.92	64.79	62.12	65.92	64.16
TiO2	0.28	0.05	0.32	0.03	0.43	0.46	0.02	0.23	0.16	0.60	0.77	0.66	0.50	0.52	0.53	0.63	0.85	0.59	0.71
Al2O3	14.37	14.42	16.59	15.57	15.85	15.90	14.14	15.09	14.90	15.31	18.29	15.85	11.64	12.37	11.60	16.73	16.77	16.23	16.67
Fe2O3*	2.49	0.61	2.48	2.45	3.28	3.52	0.82	1.62	1.19	5.64	7.20	6.25	3.69	4.74	4.07	5.87	6.89	5.12	6.35
MnO	0.07	0.10	0.07	0.96	0.06	0.07	0.15	0.03	0.03	0.08	0.14	0.10	0.05	0.06	0.15	0.12	0.12	0.13	0.11
MgO	1.11	0.21	1.25	0.34	1.27	1.33	0.35	0.86	0.65	2.76	2.94	2.69	1.46	2.03	1.80	2.74	2.88	2.26	2.77
CaO	2.12	0.50	2.75	0.72	2.68	2.97	0.43	2.50	2.15	0.59	0.35	0.98	0.97	0.99	1.85	0.59	0.75	0.88	0.87
Na2O	3.55	3.88	4.53	3.71	4.25	4.42	4.17	5.02	5.48	1.97	1.74	1.98	4.01	3.06	2.33	2.36	2.21	2.24	2.14
K2O	2.38	3.96	1.96	3.45	1.64	1.90	3.94	1.18	1.05	3.90	5.07	4.08	1.15	1.96	2.03	4.15	4.26	4.08	3.87
P2O5	0.15	0.24	0.39	0.27	0.24	0.29	0.34	0.10	0.12	0.18	0.18	0.19	0.22	0.17	0.19	0.20	0.18	0.25	0.21
LOI	0.46	0.87	0.76	0.41	0.99	0.78	0.31	0.36	0.61	2.43	2.83	1.49	1.71	1.57	0.87	2.28	2.01	1.79	1.19
total	99.23	99.97	100.68	99.75	99.00	98.70	100.36	96.29	100.22	99.20	99.21	99.05	99.18	99.34	99.34	100.46	99.02	99.48	99.06
Ba	347	54	119	40	146	133.5	7	111	5	306	n/d	400	165	170	199	308	404	458	396
Rb	178	366	92.3	114.5	85.5	110	109	64	57	159.7	23	146	38.3	81.3	98	210	194.2	158.1	214.1
Sr	145	0	165.7	16.2	177.5	199	4.2	551	473	41.8	167	104	92.1	94	175	82	88.7	105.3	81.2
Zr	142	22	108.7	133.5	134	164	22.5	166	104	160	423	178	227.1	157	223	147	176.6	181	202.3
Y	28	18	13.9	9.3	11.6	15.4	2.9	14	14	28.9	32	37	27.5	29.7	35	34	34.4	27.9	32.6
Nb	9	14	13.2	0.3	9.7	12.7	0.4	7	8	14.5	8	14	12	12.6	12	12	17.4	15.7	16.9
U	2	0	1.3	3.5	1.26	1.3	2.8	n/d	n/d	2.3	n/d	2	2.6	2.6	n/d	2	3.8	3.5	3.4
Th	5	1	3	1.2	4.6	4.58	0.4	n/d	n/d	13.1	5	2	10.1	12.1	6	10	16	11.5	15.6
Co	81	89	84.1	76	59	68.4	149.3	77	86	45.9	96	27	85.2	66.1	75	59	55.9	69.6	64.2
V	58	8	38	<8	47	47	11	35	23	87	32	123	56	66	88	128	103	86	108
La	–	–	12.6	2	16.6	17.7	1	–	–	34.2	–	–	31.9	33.2	–	–	39.1	33.4	41.6
Ce	–	–	27.5	3.6	34.6	36.9	2.2	–	–	75	–	–	70.1	70.6	–	–	85.8	73	92.7
Pr	–	–	3.48	0.44	4.15	4.44	0.24	–	–	8.54	–	–	8.04	8.07	–	–	9.88	8.41	10.6
Nd	–	–	12.6	1.6	15.8	17.1	0.8	–	–	33.5	–	–	30.4	29.4	–	–	36.7	33.1	39.5
Sm	–	–	2.5	0.49	3.16	3.49	0.26	–	–	6.55	–	–	6.07	5.83	–	–	7.08	6.14	7.72
Eu	–	–	0.86	0.08	1.04	1.09	<0.02	–	–	1.2	–	–	1.09	1.15	–	–	1.22	1.2	1.45
Gd	–	–	2.34	0.45	3.05	3.4	0.23	–	–	5.39	–	–	5.16	5.1	–	–	6.05	5.35	6.77
Tb	–	–	0.43	0.15	0.46	0.56	0.07	–	–	0.93	–	–	0.88	0.88	–	–	1.01	0.91	1.14
Dy	–	–	2.44	1.09	2.49	3.13	0.49	–	–	5.09	–	–	5.03	4.81	–	–	5.74	5.06	6.16
Ho	–	–	0.49	0.3	0.46	0.6	0.09	–	–	1.05	–	–	1.03	1.02	–	–	1.19	0.99	1.25
Er	–	–	1.53	1.14	1.29	1.65	0.31	–	–	3.11	–	–	2.91	2.91	–	–	3.35	2.85	3.65
Tm	–	–	0.23	0.31	0.18	0.24	0.07	–	–	0.49	–	–	0.46	0.45	–	–	0.57	0.46	0.57
Yb	–	–	1.48	2.68	1.08	1.5	0.58	–	–	2.98	–	–	2.65	2.75	–	–	3.29	2.58	3.46
Lu	–	–	0.22	0.43	0.16	0.22	0.1	–	–	0.43	–	–	0.39	0.4	–	–	0.5	0.39	0.51
Hf	–	–	3.3	5.8	3.2	3.9	0.9	–	–	4.6	–	–	6.5	4.4	–	–	5.3	5.3	5.1
Ta	–	–	1.7	0.2	1	1.2	0.2	–	–	1.2	–	–	0.9	1	–	–	1.5	1.2	1.1

they show higher SiO_2, Na_2O and CaO and lower Al, Ti, Fe, Mg and K_2O. The aluminum saturation index (A.S.I. = molar $Al_2O_3/CaO + Na_2O + K_2O$) of metapelites range from 1.6 to 2.1, whereas in metapsammites it is below 1.5. Major elements and some trace elements such as TiO_2, Al_2O_3, (FeOt + MgO), K_2O, and Rb decrease and CaO, Na_2O and Ba increase with increasing SiO_2 (Figs. 5 and 6). The contents of Y, Hf, Zr and REE do not show clear correlation with SiO_2.

4.2. Metatexite migmatites

Compared with metasedimentary rocks, metatexites are poor in SiO_2 and rich in Al_2O_3 TiO_2, FeO_t, MgO, Rb, V, Nb, Y, and Zr. This tendency is more accentuated in melanosome and Crd–Kfs metatexite samples reflecting high modal amounts of ferromagnesian phases such as cordierite and biotite. Metapelites and metatexite migmatites show similar multi-element patterns (Fig. 7). High contents of Zr, Th, Nb and REE reflect significant amount of accessory minerals. The leucosomes in the metatexite migmatites are usually trondhjemitic and enriched in SiO_2, CaO, Na_2O and K_2O, although they are depleted in K_2O compared with most leucogranites (Fig. 5). Leucosomes are also Sr- and P-rich and display strong depletion of total REE contents (≈40 ppm), Nb, Y, Th, U, K, Rb and Zr relative to metasedimentary rocks and metatexite migmatites. The Ba contents are extremely variable (≈200 to 900 ppm) and do not show a clear tendency with silica. Various leucosomes display a markedly positive Eu anomaly ($Eu/Eu^* = 1.06$–2.37) suggesting feldspar accumulation and display low La/Lu_N ratios (3.93–8.57). Metatexite leucosomes are the samples with the lowest total REE contents (Fig. 8e). In contrast, melanosomes exhibit multi-element patterns similar to metapelites and metatexites, although REE, Zr, Th, Nb, Y and Rb contents are slightly higher (Fig. 7). The melanosomes display modest variation in silica (62 to 64 wt.%) and compared to leucosomes they are enriched in Al_2O_3, TiO_2, FeO_t, MgO, K_2O, ΣREE, Rb, V, Nb, Y, and Zr and depleted in CaO, Na_2O, Sr, and P (Figs. 5–8). The REE pattern is virtually identical in all melanosome

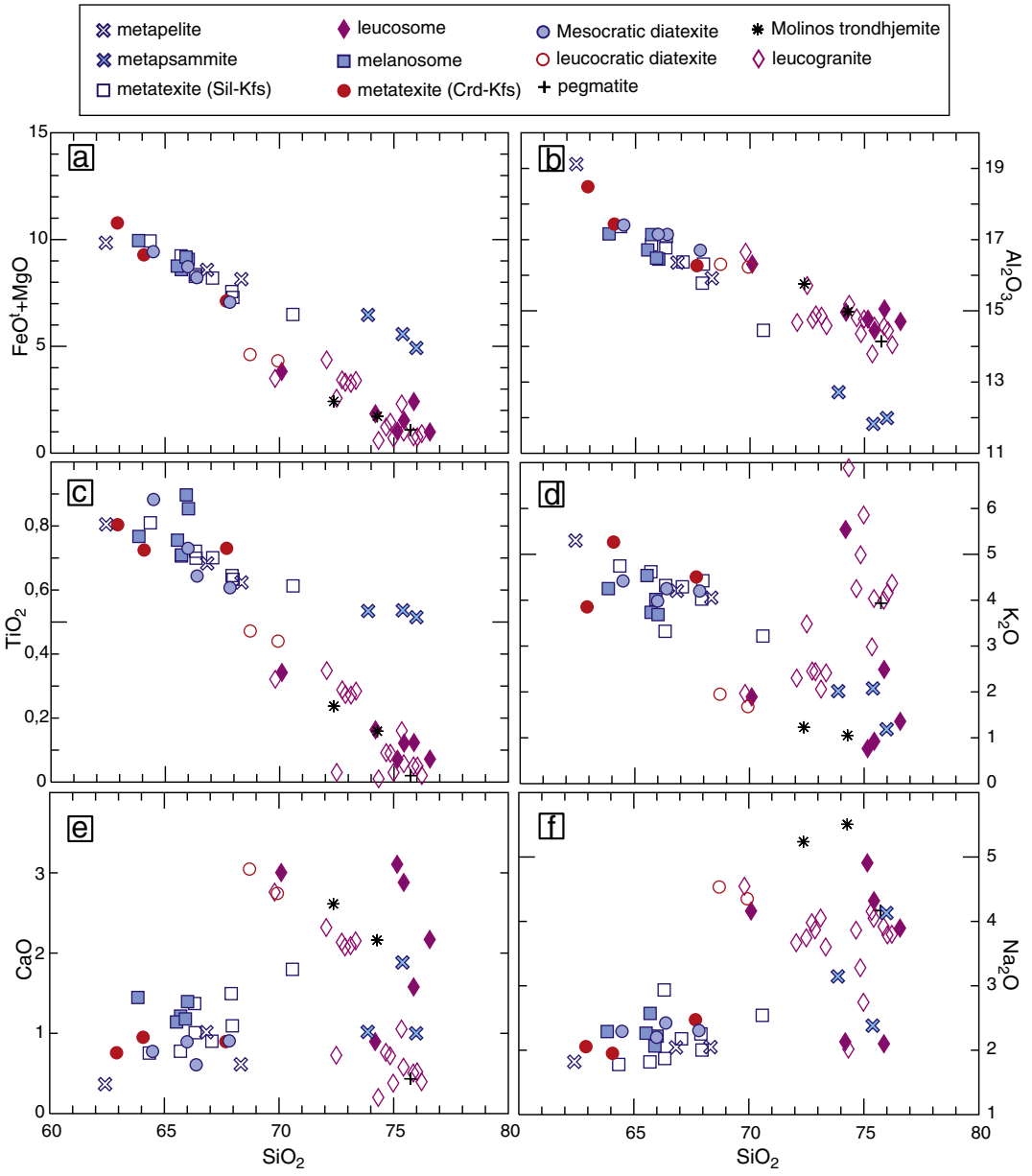

Fig. 5. Harker diagrams of major element compositions show the relations between metasedimentary rocks (Puncoviscana Formation), migmatites (metatexites and diatexites) and granites. a) (FeO_t + MgO) Total iron as FeO; b) Al_2O_3; c) TiO_2; d) K_2O; e) CaO; and f) Na_2O. Recalculated to 100 wt.% anhydrous.

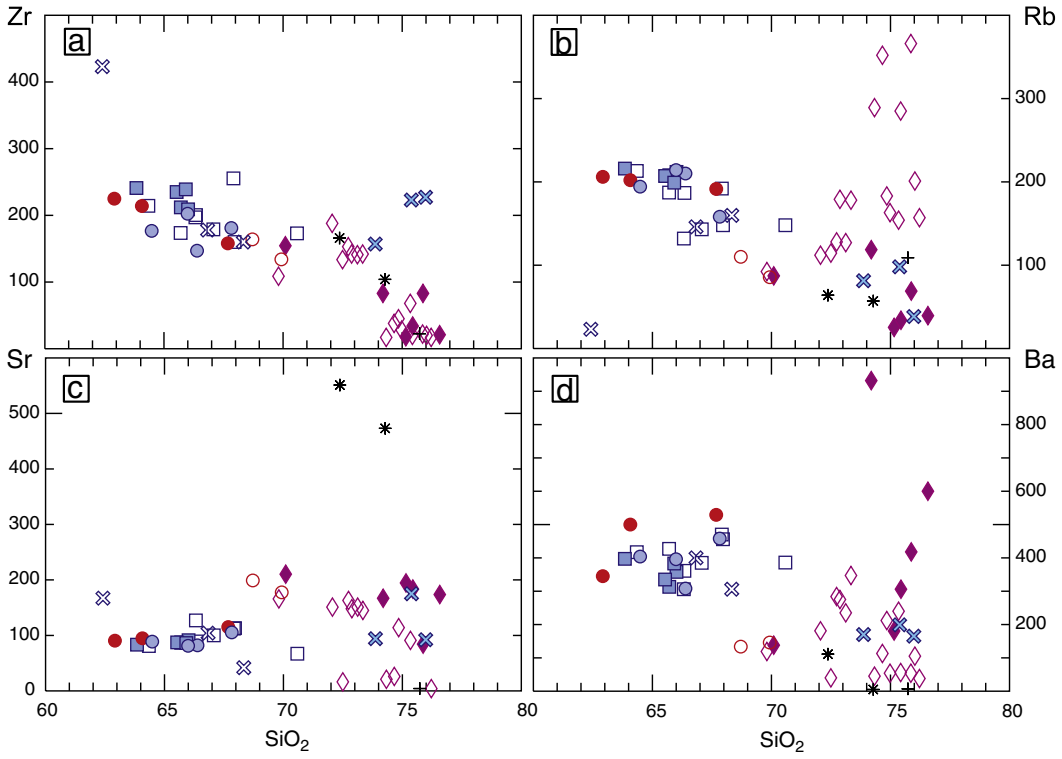

Fig. 6. Harker diagrams compare trace element compositions of metasedimentary rocks, migmatites (metatexites and diatexites) and granites. a) Zircon b) rubidium c) strontium and d) barium. Symbols are as in Fig. 5.

samples, showing Eu anomaly markedly negative ($Eu/Eu^* = 0.54$; Fig. 8c). The average of total REE content in melanosomes is 225 ppm, nearly six times greater than that of leucosomes.

4.3. Diatexites

Leucocratic diatexites display intermediate multi-element patterns between leucosomes and melanosomes (Fig. 7). The REE patterns of these diatexites do not exhibit Eu anomaly ($Eu/Eu^* \approx 1$) and the La/Lu_N ratios range between 8.62 and 11.12 which defines a moderate slope. The leucocratic diatexites, same as the leucosomes, are CaO-, Na_2O- and Sr-rich and have low Rb/Sr ratios (0.1–0.8), although compared to them, they are more rich in (Fe_t + Mg), Al, Ti, Rb and Zr (Figs. 5 and 6). The mesocratic diatexites are less siliceous than leucocratic diatexites and are enriched in Al_2O_3, TiO_2, FeO_t, MgO and the other trace elements (e.g. Ba, Rb, Th, and total REE) except for Sr and P (Figs. 5 and 6). The multi-element patterns of mesocratic diatexites closely resemble those of metatexite migmatites, melanosomes and metapelites showing negative Ba, Nb, Sr, P and Ti anomalies (Fig. 7a–d).

4.4. Leucogranites, trondhjemites and pegmatites

Granitoids are silica-rich and moderately peraluminous rocks (A.S.I = 1.06 to 1.4). Modally, the granites range from leuco-tonalites to syenogranites. Following the normative (Ab–An–Or) classification for felsic plutonic rocks proposed by Barker (1979), most of the samples fall within granite and trondhjemite fields (Fig. 9). The silica content in leucogranites and pegmatites is high, ranging from 70 to 76 wt.%; CaO is normally <1 wt.% and the concentration of K_2O and Na_2O is generally around 4 wt.%. The concentrations of Al_2O_3, TiO_2, (FeO_t + MgO), CaO, Sr and Zr show negative correlation with SiO_2 (Figs. 5 and 6). The content of Rb range from 100 to 350 ppm and the Sr is low <200 ppm. Leucogranites are the samples with more varied large-ion-lithophile (K, Sr, and Rb) and REE contents (Figs. 7e and 8e). On the other hand, the Molinos trondhjemite in comparison with the leucogranites has high concentration of CaO and Na_2O and low K_2O. Comparatively these rocks are extremely enriched in Sr (≈500 ppm) and depleted in Rb (≈50 ppm); these features are shared by other trondhjemitic plutons along the Famatinian belt (Galliski et al., 1990; Méndez et al., 2006). Except for the extreme concentration of Sr, the chemistry of trondhjemite resembles that of leucocratic diatexites and some leucogranites.

5. Geochronology

U–Pb ratios were determined in individual zircon grains using laser ablation ICP-MS method. To assess the age of the anatectic event in this region, zircons from a mesocratic diatexite migmatite (sample MO102/08), a trondhjemite (sample MO45) as well as a leucosome from a metatexite migmatite (sample MO106), were analyzed (Fig. 10; Table 2). In addition samples from the low grade metasedimentary rocks (MO6/09) and mesocratic diatexite sample (MO102/08) were chosen in order to constrain the inheritance pattern of the protolith. Details of the sample preparation and analytical procedures are described in Appendix A. The sample locations are shown in Fig. 2.

The internal texture of the zircons was investigated by backscattered images. Most zircons are small, around 100 to 150 μm long, and have aspect ratios of 2–3. Many zircons from the diatexite have rounded cores surrounded by more or less euhedral rims. A few zircon grains display cores with a well defined fine euhedral zoning, although the cores with irregular zoning or without zonation are more frequent. We interpreted the rounded cores as inherited zircons and the overgrowths or rims as magmatic zircon grown during crystallization of anatectic melt.

5.1. Crystallization ages (U–Pb zircon)

The diatexite (MO102/08; Table 2) yielded a crystallization age of 464 ± 5 Ma (2σ errors). This age is indicated by most concordant

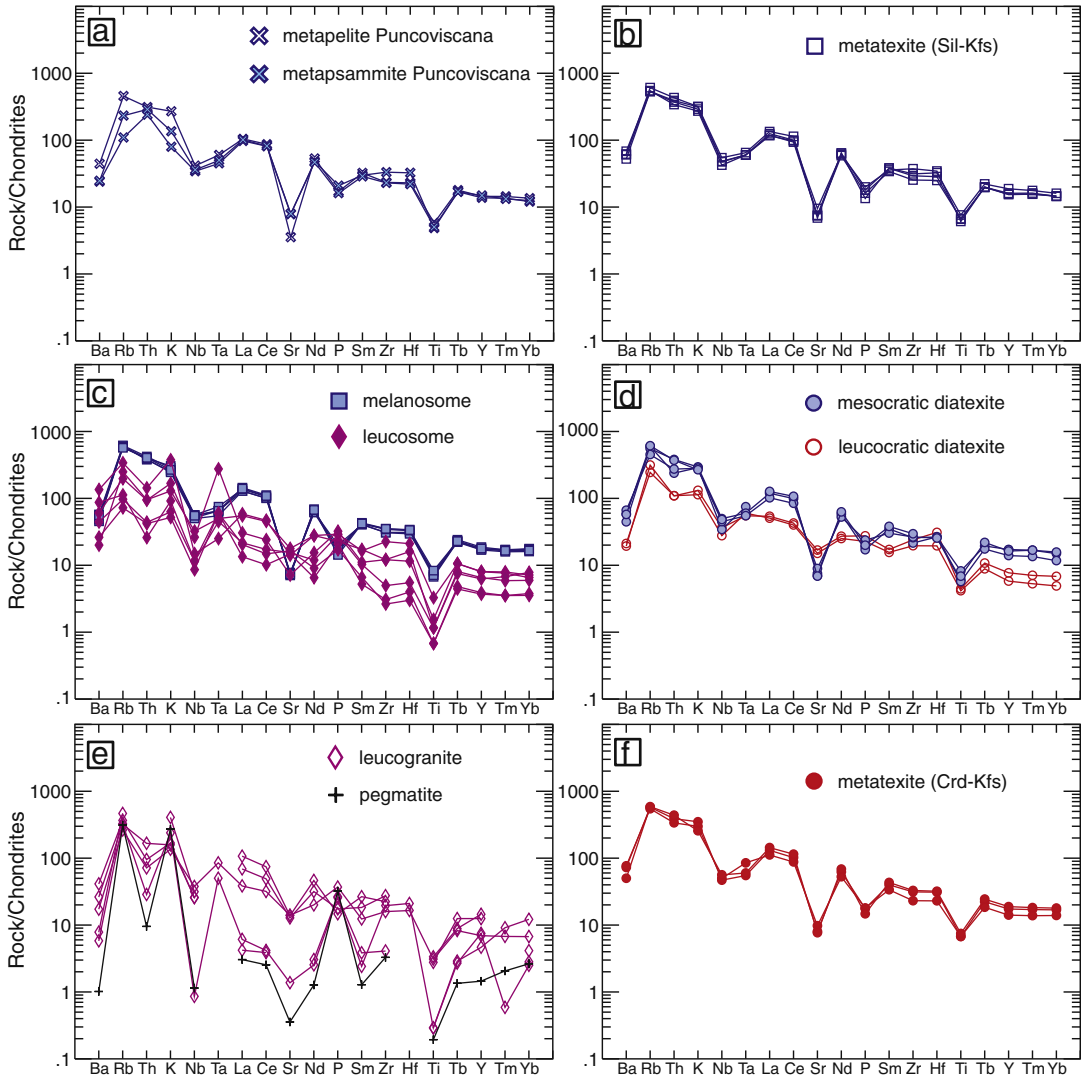

Fig. 7. Multi-element diagrams normalized to chondrite values of Thompson (1982). See text for discussion.

magmatic rim analyses (Fig. 10a) and it is equivalent to that determined on monazite by Lork et al. (1989) for the La Angostura granite (462 ± 1 Ma). The metatexite leucosome (sample MO106), was analyzed by Sola et al. (2010) yielding 466 ± 3 Ma (Fig. 10c). For Molinos trondhjemite (MO45; Table 2) a slightly older crystallization age of 473 ± 5 Ma (2σ errors) was obtained (Fig. 12b). The spread along the concordia curve observed in all our samples is interpreted as inheritance derived from the metasedimentary source.

All the obtained ages are identical within the analytical precision and overlap with regional data for the Famatinian high grade metamorphic peak and associated granitic plutonism 480–460 Ma (Fig. 1, e.g. Büttner et al., 2005; Ducea et al., 2010; Lork et al., 1989; Pankhurst et al., 2000.).

5.2. Inherited ages

There are no records of inherited age distribution in high-grade metamorphic rocks in the region. The distribution of inherited ages in these high-grade anatectic rocks and the comparison with detrital zircon ages from very low grade Puncoviscana metasediments are helpful to understand whether this sedimentary sequence is actually the protolith of migmatites. The results are shown in Fig. 11. The ages were calculated from $^{206}Pb/^{238}U$ ratios. Two zircon populations dominate the age frequency in the low grade metasediments and diatexite migmatites; one of Late Neoproterozoic–Early Cambrian age (520–650 Ma) and the other of Early Neoproterozoic–Late Mesoproterozoic age (1200–900 Ma). Variations in the proportion of each population are in agreement with internal variations of the Puncoviscana basin at different geographic localities (see Adams et al., 2008). Zircon ages older than 2000 Ma are observed in both analyzed samples with the oldest age of 2661 Ma found in the metasedimentary sample, very close to the 2625 Ma age found in the diatexite sample. The inheritance patterns of the new samples are in excellent agreement with published data of Puncoviscana metasedimentary rocks at Rancagua and Rio Choromoro localities (Fig. 11, Adams et al., 2008), which strongly supports derivation of migmatites from Puncoviscana metasedimentary rocks.

6. Nd–Sr isotope data

Strontium and neodimium isotope data were acquired on 16 samples including metasedimentary rocks, migmatites and leucogranites from Sierra de Molinos. The isotopic compositions are shown on Table 3. Analytical procedures are detailed in Appendix A. The initial Sr and Nd isotopic ratios were calculated for 470 Ma, considered as the age of granitic magmatism and migmatization (Fig. 12). All the samples are characterized by continental crust isotopic compositions. The initial $^{87}Sr/^{86}Sr$ ratio in low grade metasedimentary rocks varies widely

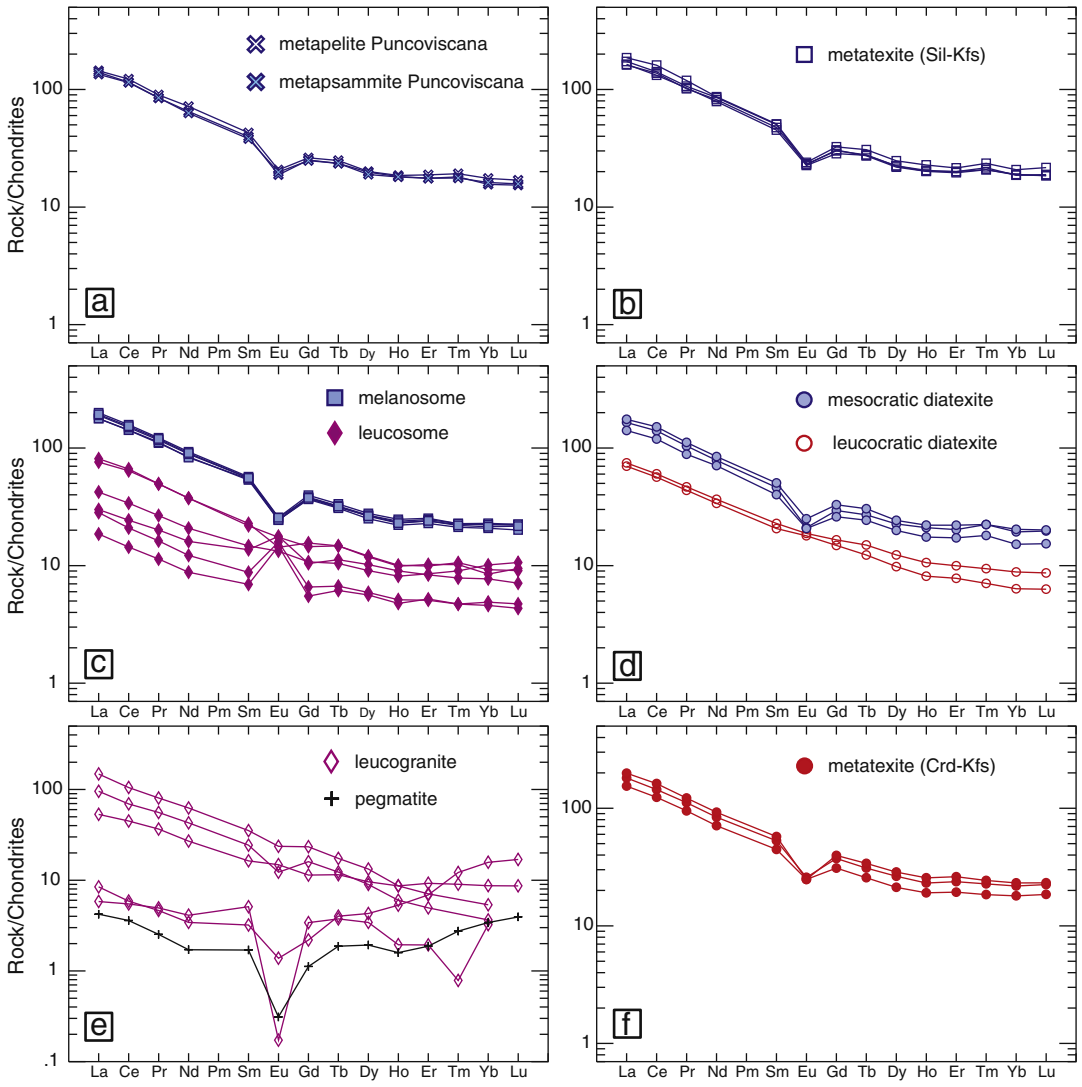

Fig. 8. Rare earth diagrams normalized to chondrite values of Sun and McDonough (1989). See text for discussion.

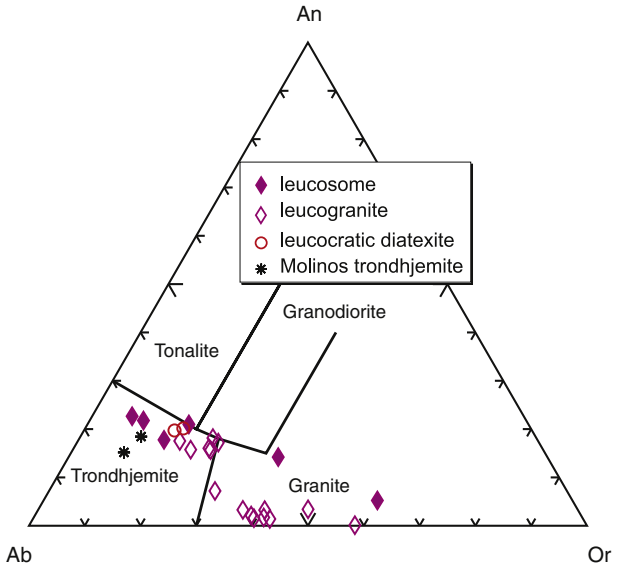

Fig. 9. Normative anorthite–albite–orthoclase classification diagram for silicic rocks proposed by Barker (1979). See text for discussion.

from 0.80036 to 0.71830, in contrast, they exhibit narrow εNd_t values (−6.7 to −7.2) similar to metatexite and diatexite migmatites (see Fig. 12). The initial $^{87}Sr/^{86}Sr_{(470\ Ma)}$ ratios of leucogranites range from 0.70893 to 0.71790, this last value being very similar to that obtained in the trondhjemitic leucosome (MO53) $^{87}Sr/^{86}Sr_{(470\ Ma)} = 0.71910$. These rocks, which represent anatectic melts, also display a varied εNd_t when compared to their metasedimentary protoliths with εNd_t between −7.81 and going up to −3.02 in the metatexite leucosome.

The initial Sr ratios and εNdt values are comparable to those previously published for Early Paleozoic granites and metamorphic rocks in the region (Franz et al., 2006; Lucassen et al., 2000, 2001 and references therein). We interpret this isotopic data in terms of old crust reworking instead of reflecting mixing of a juvenile component. The field relationships are the strongest evidence to support the genetic link of these rocks with the granites and leucosomes as anatectic products of metasedimentary rocks. Nevertheless, further detailed isotopic studies are needed to fully corroborate this interpretation

7. Discussion

The strength of the geochemical approach is that it can provide evidence of the processes that occur during the evolution (melting, segregation and crystallization stages) of partially melted terranes, by

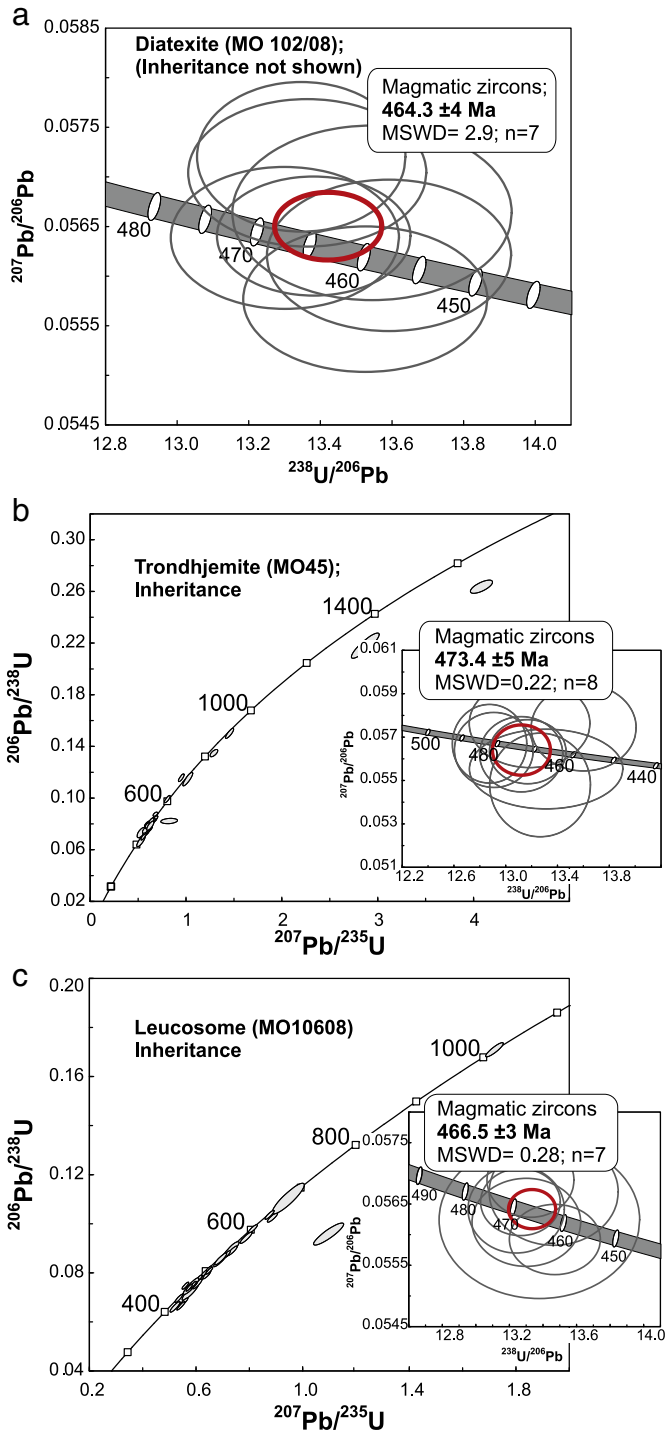

Fig. 10. Crystallization ages obtained for Sierra de Molinos rocks. a) Tera-Wasserburg diagram for zircons from a mesocratic diatexite migmatite (sample 102/08). b) Concordia and Tera-Wasserburg diagrams for zircons from a trondjhemite (sample MO 45). c) Concordia and Tera-Wasserburg diagrams for zircons from a leucosome of a metatexite migmatite (sample MO106/08); ellipses depict 2 s errors.

enabling particular components to be recognized, e.g. protolith, residuum and melt fractions (e.g. Milord et al., 2001; Sawyer, 1999; Solar and Brown, 2001).

7.1. The protolith composition

On the basis of field relationships, mineral assemblage and geochemical arguments, metapelites can be identified as the protolith of migmatites. It is well established that hydrated rocks progressively devolatilize during prograde metamorphism, and could simultaneously lose some major and trace elements (e.g. Ague, 1994). However, contact aureoles and some regional metamorphic terranes in which low grade country rocks were rapidly heated and melted, may be an exception if the fluids and any trace elements released by prograde devolatilization remain in the rocks and were incorporated wholesale into the migmatites (see Sawyer, 2008, Section 6). Apart from devolatilization (loss of H_2O and CO_2) we assume a progressive syntectonic and effectively isochemical metamorphism at sub-solidus conditions. The metapelitic rocks collected in Molinos (samples MO10408 and MO40) contain around 15–16 wt.% Al_2O_3, 64–66 wt.% SiO_2, with 4 wt.% of K_2O, ~2 wt.% Na_2O, 2–3 wt.% MgO, 5–6 wt.% FeOt and <1 wt.% of CaO. This composition is in perfect agreement with the average of Puncoviscana Formation metapelites, as can be seen from published data in Becchio et al. (1999), Lucassen et al. (2001) and DoCampo and Guevara (2005). There is only one sample (MO25) that deviates from the average composition due to anomalous high contents of Al_2O_3, (FeOt + MgO), Zr, MnO (1.4 wt%) and low silica and Rb. In contrast to metapelites, metapsammites are silica- and Ca–Na-rich according with the high contents of quartz and plagioclase. The low Al_2O_3, (Fe + Mg) and K_2O concentration reflect relatively low phyllosilicates contents. These rocks are too silicic to represent the protolith of migmatites and usually are found as competent layers or rafts surrounded by neosome. The mineralogy of high grade rocks in Molinos, rich in biotite, sillimanite, cordierite and K-feldspar, requires necessarily a metapelitic relatively Al–Mg-K-rich protolith and the samples MO10408 and MO40 may well represent this “fertile” protolith.

7.2. Estimating the degree of partial melting in migmatites

Having assessed the probable protolith composition it is possible to understand the variation diagrams in terms of gain or loss of components that are compatible with the quartz–feldspatic anatectic melt (e.g. SiO_2, CaO, Na_2O, Sr, and Rb) and those elements compatible with the melanocratic residuum left after partial melting (e.g. TiO_2, FeO_t, MgO, Al_2O_3, Zr, and Nb) (Figs. 5 and 6). The relationship between the known compositional endmembers of the partial melting process i.e., protolith, anatectic melt, solid residuum and the degree of partial melting can be estimated quantitatively by means of mass balance calculation expressed as:

$$C_0 = C_s(1-F) + C_L F$$

where C_0 represents the composition of the source or protolith (major elements in wt.% and trace elements in ppm) before partial melting; C_s is the composition of the solid residuum (melanosome); C_L is that of the melt (leucosome) and F is the degree of partial melting expressed in wt.% basis (e.g. Prinzhofer and Allegre, 1985). The degree of partial melting (F) to produce a leucosome can be estimated if the source (C_0), leucosome (C_L), and residue (C_s) compositions are known. This calculation ideally assumes that 1) the leucosomes do not contain significant residue and 2) the leucosomes do not undergone fractional crystallization or crystal accumulation. Such conditions are usually difficult to meet in migmatitic terranes (e.g. Brown, 2001; Sawyer, 2008; Solar and Brown, 2001 and references therein) (see next section). An alternative approach is to use the elements which are strongly concentrated into the residue (e.g. TiO_2, Fe_2O_3, MgO, Zr, V and Nb) such that the mass balance calculation [$C_0 = C_s\ (1 - F) + C_L F$] reduces to $F = (C_S - C_0)/C_s$. Melting is then estimated using source rock and residuum (melanosomes) compositions only (Sawyer, 1991). In this study, the composition of metapelite MO10408 is used for C_0 and melanosomes Mel1-2–3–4 are taken for residuum composition (C_s). Results obtained for degrees of partial melting are given in Table 4. The calculated degrees of partial melting (F) in the metatexite migmatites of the Molinos area range from 0.18 to 0.23.

Table 2
Crystallization ages. U–Pb zircon (ICP-MS) laser ablation data.

Spot	$^{207}Pb/^{206}Pb$	2 s(%)	$^{207}Pb/^{235}U$	2 s(%)	$^{206}Pb/^{238}U$	2 s(%)	Apparent ages (Ma)					
							$^{207}Pb/^{206}Pb$	2 s(Ma)	$^{207}Pb/^{235}U$	2 s(Ma)	$^{206}Pb/^{238}U$	2 s(Ma)
Sample MO10208 mesocratic diatexite												
12_Z3	0.05639	1.0	0.58459	2.2	0.07519	2.0	467.7	22.9	467.4	8.3	467.3	8.8
19_Z7	0.05640	0.9	0.58123	1.9	0.07474	1.6	468.3	19.2	465.3	7.0	464.6	7.4
30_Z12	0.05704	1.1	0.58860	2.3	0.07484	2.0	493.1	23.4	470.0	8.6	465.2	9.1
31_Z12	0.05577	1.1	0.56863	2.3	0.07394	2.1	443.4	23.8	457.1	8.5	459.9	9.1
62_Z26	0.05621	1.1	0.57031	2.3	0.07358	2.0	460.8	24.5	458.2	8.6	457.7	9.0
86_Z39	0.05720	1.1	0.59101	2.1	0.07493	1.8	499.4	23.6	471.5	7.8	465.8	8.0
31_Z15	0.05664	1.3	0.57665	2.7	0.07384	2.3	477.6	28.0	462.3	9.9	459.2	10.4
Sample MO45 trondhjemite												
11_Zr4	0.05743	2.8	0.58229	3.7	0.07353	2.4	508.3	61.0	465.9	13.8	457.4	10.7
18_Zr7	0.05553	2.7	0.57523	4.5	0.07513	3.6	433.8	58.7	461.4	16.6	467.0	16.3
23_Zr9	0.05633	2.1	0.58978	2.8	0.07594	1.8	465.3	46.6	470.7	10.6	471.8	8.4
40_Zr18	0.05621	2.5	0.59085	3.2	0.07623	2.0	460.8	54.8	471.4	12.0	473.6	9.1
42_Zr20	0.05670	2.6	0.60716	3.2	0.07767	1.8	479.7	56.5	481.8	12.1	482.2	8.5
43_Zr21	0.05762	2.9	0.60269	4.1	0.07586	2.9	515.5	61.8	478.9	15.4	471.3	13.1
53_Zr26	0.05642	2.5	0.60264	3.2	0.07747	1.9	468.7	54.4	478.9	12.0	481.0	8.9
48_Zr23	0.05480	3.6	0.56966	4.3	0.07539	2.4	404.2	77.7	457.8	15.7	468.5	10.8
Sample MO106/08 leucosome (metatexite)												
11_Z5	0.05620	1.0	0.58268	2.2	0.07519	2.0	460.4	23.1	466.2	8.4	467.4	8.9
13_Z6	0.05670	1.2	0.58067	2.6	0.07428	2.3	479.8	27.6	464.9	9.9	461.9	10.4
16_Z7	0.05641	1.0	0.58751	2.0	0.07553	1.8	468.6	22.7	469.3	7.7	469.4	8.0
32_Z18	0.05624	1.9	0.57972	4.1	0.07476	3.6	462.0	41.2	464.3	15.2	464.7	16.3
47_Z24	0.05689	0.9	0.58873	1.8	0.07506	1.6	487.2	19.1	470.1	6.8	466.6	7.1
48_Z24	0.05653	0.8	0.58764	1.7	0.07539	1.5	473.4	17.4	469.4	6.2	468.5	6.6
55_Z27	0.05592	0.8	0.57250	1.8	0.07425	1.6	449.4	18.5	459.6	6.8	461.7	7.3

Many metatexites show chemical attributes comparable to that of melanosomes, with some depletion in granitic component and represent presumably a mixture of solid residues and leucosome; where the leucosome may consist of some mixture of residual felsic minerals, early crystallized felsic minerals (cumulates) and possibly unextracted melt (e.g. Brown, 2001). Because migmatitic terranes may constitute the probable source areas of leucogranites it is interesting to investigate and quantify the *degree of melt extraction* underwent by metatexite migmatites. For this, the whole-rock compositions of metatexite migmatites are used for C_s. In this calculation *F* does not represent the degree of partial melting in the metatexites but represent the degree of melt extraction from these migmatites. Results are presented in Table 5, ranging from 0.13 to 0.25. These calculations indicate that the majority of metatexites exhibit a residual or melt-depleted bulk composition, with the highest degree of melt extraction obtained for sample ResB (Table 5). As some melt remained in metatexites, the degree of partial melting must exceed the degree of melt extraction, which implies that it could be higher than 0.25 in some places.

7.3. The initial melt composition

The determination of the initial melt composition is critical to elucidate the evolution of anatectic systems, because the composition of melt may change due to a variety of factors (e.g. fractionation, residue contamination). Leucosomes, leucocratic diatexites, leucogranites, etc., that could represent initial anatectic melts are compared with experimental melt from partial melting experiments of metasediments (Fig. 13), under conditions similar to those inferred for the Molinos area (<800 °C and <6 kbar Patiño Douce and Harris, 1998). During fractional crystallization, the early-crystallized phases are separated from the fractionated or evolved liquid. The samples that represent accumulations of the early-formed minerals (cumulates) will plot nearer the plagioclase–quartz line, whereas the samples of fractionated melts will plot toward the opposite direction, near the quartz–orthoclase line (Fig. 13). Fig. 13 shows that many leucogranite samples have compositions close to the experimentally generated melt. Most of the leucosomes, leucocratic diatexites and trondhjemites, on the contrary, show compositional trend towards the cumulates. These rocks may contain some cumulate material of either restitic or magmatic origin and, therefore, do not seem to represent initial anatectic melts. Patiño Douce and Harris (1998) suggested that initial trondhjemitic melts (Ca–Na-rich) could also form as a consequence of low temperature (700–750 °C) H_2O-fluxed melting of K-rich metasedimentary source rocks. However, given the limited amount of water-rich metamorphic volatile that can be stored in rocks at upper amphibolite facies conditions; we expect that melting will be dominated by dehydration melting instead of H_2O-fluxed melting. Moreover, leucosomes and neosomes containing anhydrous peritectic minerals, such as sillimanite, K-feldspar and cordierite, are indicators that dehydration melting has taken place (e.g. Spear et al., 1999).

7.4. Chemical differentiation during partial melting

The geochemical evidence suggests that the compositional variation within the anatectic rocks from Molinos can be interpreted as a result of 1) variable degrees of melt–residuum separation and 2) fractional crystallization of the anatectic melt.

The influence of these two processes is best shown in bivariant diagrams (e.g. Fig. 14) in terms of vectors for initial melts, residual compositions and for ideal mineral phases (albite, anothite, orthoclase, and quartz). We consider the residue or "restite" as a mixture of unmelted and peritectic minerals remaining after a melt-producing-reaction. The sample ResB is selected as a contaminant because it exhibits a marked melt-depleted character in terms of chemistry and mineralogy, although, similar results are obtained using other residual compositions. This sample is composed largely of biotite, cordierite, K-feldspar (microcline–microperthite), quartz and plagioclase. The vectors for mineral compositions show accumulation of a given phase indicating trends for either fractionated melts (K-feldspar-rich) or cumulates (plagioclase-rich).

The metatexites, as expected, plot along the mixing lines between experimentally generated melt and residue, indicating that segregation processes were dominant with variable degrees of melt extraction (Fig. 14a). The compositions of mesocratic diatexites are more restricted than metatexites and plot near the likely protolith (metapelites: MO104/08 and MO40), i.e. do not show a significant gain or loss of granitic or residual components. Experimental studies show that melts formed by

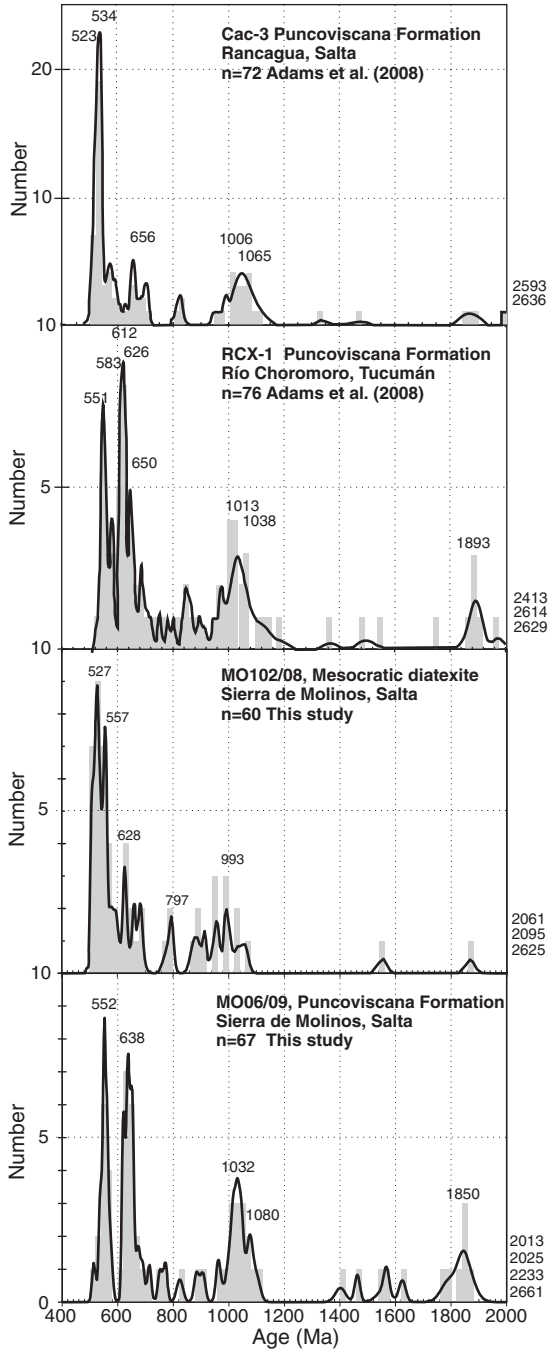

Fig. 11. Age distribution for inherited zircons in the mesocratic diatexite migmatite and the very low grade metasedimentary rocks compared with zircon ages from Puncoviscana sequence (Adams et al., 2008). Note the agreement in age distribution between the migmatites, the low grade rocks and detrital zircons of Puncoviscana Formation (Rancagua and Río Choromoro localities).

partial melting of crustal material at T ≤ 800 °C have relatively low FeO and MgO contents with (FeO + MgO) <2 wt.% (e.g. Patiño Douce and Harris, 1998). In leucocratic diatexites the sum of FeO_t and MgO is approximately 5 wt.%, well above the contents of experimentally generated melts (Fig. 14a). These high values can only be explained by contamination with a residuum that is rich in ferromagnesian phases. Petrographic observations show that the mafic mineral controlling the iron and magnesium concentrations in leucocratic diatexites is biotite. Additionally, the contents of sodium and calcium in these diatexites are high (Na_2O + CaO ≈7 wt.%) and residue contamination alone cannot explain this behavior; the fractionation of an evolved liquid (K-feldspar- and quartz-rich) is also required. Part of leucogranites follows this trend although less marked (Fig. 14b, c). The leucosomes, except for sample MO53, do not show significant influence of residuum contamination, but they do for fractionation. Most of the leucosomes represent cumulates of sodic plagioclase, with the exception of sample MO106, which has an evolved K-feldspar-rich composition. Various leucogranite samples and the garnet-bearing pegmatite (MO32), with low (FeO_t + MgO) <2 wt.%, (CaO + Na_2O) around 5 wt.% and K_2O ≈4 wt.%; have compositional character very close or equivalent to the experimentally generated melt (Fig. 14).

The effect of fractional crystallization and melt–residuum separation can also be examined in terms of the trace elements distribution. Because Eu is highly compatible with crystallizing feldspar (Bea, 1996), early-formed feldspar cumulates show positive Eu anomalies, whereas the respective fractionated melts are relatively depleted in Eu and display negative Eu anomalies. In Molinos, the plagioclase-rich leucosomes with the lowest biotite contents (samples Leu1-2–3–4) have prominent positive Eu anomalies (Fig. 8c) and low Rb/Sr (0.13–0.82) ratios, consistent with being a cumulate of early crystallized plagioclase, which is also supported by the major element evidence (e.g. Fig. 14b, c). However, other plagioclase-rich rocks with higher biotite contents (10–15 vol.%) like the leucocratic diatexites, do not exhibit positive Eu anomaly, indicative of plagioclase accumulation (Fig. 8d). Milord et al. (2001) and Solar and Brown (2001) showed that this effect could be caused by abundance of accessory phase inclusions in residual biotite, especially in metamorphic terranes where a widespread biotite breakdown did not occur. Fig. 15a shows that biotite, represented by (FeO_t + MgO + TiO_2), exerts a strong control on the abundances of zircon and monazite, represented by (Zr + Th); with the biotite-rich melanosomes containing more zircon and monazite than the biotite-free leucosomes. The entrainment of residual biotite together with inclusions of accessory phases such as zircon and monazite into the melt, will cause enrichment of total REE except for Eu. This contamination effect is modeled by simple mixing of melanosome and leucosome fractions in Fig. 15b; showing that a low fraction of biotite-rich melanosome as ~20 wt.% is enough to completely mask the original Eu anomaly, reproducing the REE patterns of leucocratic diatexites. This fraction corresponds to ≤10 vol.% of pure biotite (plus inclusions), considering the proportion of biotite in melanosomes. These apparently "unfractionated" REE patterns are documented in many biotite-bearing trondhjemite plutons from the Cachi Formation (see Méndez et al., 2006). Likewise, the inherited ages in zircons showed that a large proportion of zircon in the mesocratic diatexites is inherited from the source i.e., restitic in origin (Fig. 11). The statistically highly significant correlation between Zr concentrations and the proportions of biotite in the melt-rich rocks could be interpreted in terms of the residuum–melt separation, assuming that a significant proportion of the biotite is residual in origin, and much of the zircon was enclosed in biotite.

7.5. Transition from migmatites to anatectic granites at Sierra de Molinos

The formation and evolution of migmatitic terranes usually involve a sum of petrological processes, and the migmatites and associated anatectic granites may represent intermediate or extreme stages of such processes. The location of leucosomes at structurally controlled sites such as shears bands, interboudin partitions, fold hinges or network structures (e.g. Fig. 3c), indicates that partial melting occurred under conditions of differential stress with the melt flowing through the migmatites during deformation ("dynamic melting"; see Sawyer, 2008). This means that a low fraction of melt is required to attain melt connectivity, allowing for melt/solid segregation and for migration of the melt beyond the grain scale (e.g. Vanderhaeghe, 2009; Vigneresse et al., 1996 and references therein). The melt–residuum separation could be nearly perfect at such low melt fractions (e.g. Sawyer, 1991,

Table 3
Sr–Nd isotopic data for Sierra de Molinos rocks.

Sample	Rock type	Rb (ppm)	Sr (ppm)	$^{87}Rb/^{86}Sr$	$^{87}Sr/^{86}Sr$ *Meas.* (±2SE)	$(^{87}Sr/^{86}Sr)t$	Sm (ppm)	Nd (ppm)	$^{147}Sm/^{144}Nd$	$^{143}Nd/^{144}Nd$ meas. (±2SE)	$(^{143}Nd/^{144}Nd)t$	$\varepsilon Nd_{(0)}$	$\varepsilon Nd_{(470)}$
MO 49	Metasediment	81.3[a]	94[a]	2.51	0.73510 ± 3	0.71830	6.301	31.858	0.1196	0.512058 ± 10	0.511690	−11.3	−6.69
MO 25	Metasediment	23	167	0.40	0.80305 ± 2	0.80036	7.031	34.751	0.1223	0.512009 ± 20	0.511632	−12.3	−7.81
MO 37	Metatexite	213.1[a]	80.9[a]	7.65	0.74268 ± 3	0.69147	9.161	47.895	0.1156	0.512016 ± 13	0.511660	−12.1	−7.3
MO 26	Metatexite	132	127	3.02	0.74471 ± 2	0.72450	7.585	38.461	0.1192	0.512054 ± 17	0.511687	−11.4	−6.75
MO 39	Metatexite	148	67	6.43	0.77704 ± 3	0.73395	9.519	48.569	0.1185	0.512024 ± 8	0.511659	−12.0	−7.29
MO 44	Metatexite	148	113	3.81	0.75390 ± 4	0.72841	6.175	37.044	0.1008	0.512036 ± 9	0.511726	−11.7	−5.99
MO 38	Metatexite	187.2[a]	87.1a	6.25	0.76198 ± 3	0.72012	7.676	37.923	0.1224	0.512022 ± 11	0.511645	−12.0	−7.56
MO 51	Diatexite	194.2[a]	88.7[a]	6.37	0.75748 ± 4	0.71486	6.546	33.592	0.1178	0.512040 ± 9	0.511677	−11.7	−6.94
MO 61	Diatexite	210	82	7.43	0.73996 ± 2	0.69019	4.681	23.211	0.1219	0.511899 ± 18	0.511524	−14.4	−9.9
MO 53	Leucosome	87.2[a]	210.2[a]	1.20	0.72715 ± 3	0.71910	3.389	17.186	0.1192	0.512245 ± 6	0.511878	−7.7	−3.02
MO 35	Leucogranite	154	91	4.91	0.74311 ± 3	0.71021	2.504	9.721	0.1557	0.512310 ± 12	0.511831	−6.4	−3.94
MO 56	Leucogranite	178	145	3.56	0.73277 ± 3	0.70893	3.511	16.807	0.1263	0.512176 ± 7	0.511787	−9.0	−4.79
MO 57	Leucogranite	179	148	3.51	0.73260 ± 6	0.70911	3.208	14.928	0.1299	0.512252 ± 14	0.511852	−7.5	−3.52
MO 33	Leucogranite	183	114	4.66	0.74768 ± 4	0.71646	1.513	6.36	0.145	0.512079 ± 10	0.511633	−10.9	−7.81
MO 80	Leucogranite	127	151	2.44	0.73330 ± 2	0.71696	2.82	12.719	0.134	0.512141 ± 8	0.511728	−9.7	−5.94
MO 72	Leucogranite	92.3[a]	165.7[a]	1.61	0.72871 ± 3	0.71790	2.685	12.953	0.1253	0.512246 ± 17	0.511860	−7.6	−3.36

[a] Taken from ICP-MS analyses.

1998; Wickham, 1987) and may give rise to relatively residuum-free leucosomes and leucogranite plutons like those observed in this region. The estimates for melt extraction suggest that migmatites of this region are the result of open system processes and residual metatexites are formed as a consequence of variable degrees of melt extraction assisted by deformation (see Table 5). Additional evidences of movement and removal of melt from migmatites are: 1) layers (interpreted as former leucosome) very rich in coarse-grained peritectic cordierite; 2) leucosomes that have lost melt, on the basis of mineralogical and compositional evidence (trondhjemitic Ca–Na-rich leucosomes); and 3) abundance of peritectic minerals (cordierite, K-feldspar or sillimanite) in migmatites, with amounts of leucosomes that are too small to account for these abundances. On the other hand, a diatexite migmatite forms at the sites where the segregated melt accumulates. The mesocratic diatexites do not show evidences of restite segregation whereas the leucocratic diatexites appear to lose restite as they flow becomes more leucocratic (e.g. Milord et al., 2001; Sawyer, 1998). In a cooling stage the geochemical signature of fractional crystallization replaces gradually that of melt–residuum separation. The trondhjemites and leucocratic diatexites represent likely the early crystallizing products of melt, thus, the network defined by such melts represents transfer paths rather than melt accumulation sites. The acquired chronological data imply that the time spent above the solidus i.e. migmatization, granite extraction (segregation) and in situ crystallization of remaining melt was of several million years, at least from 472 Ma (Molinos trondhjemite) to 462 Ma (La Angostura granite).

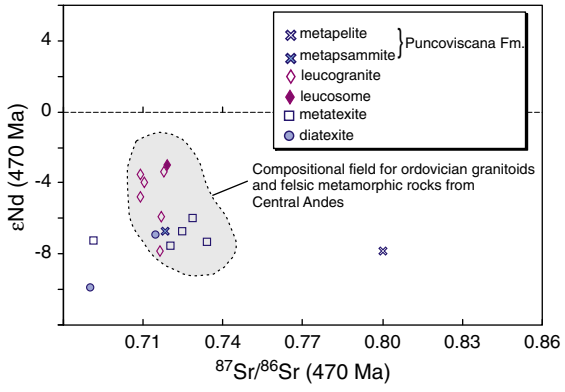

Fig. 12. Initial Sr and Nd isotope ratios of rocks from Molinos complex. Compositional field for Ordovician rocks between 21 and 27°S (see Franz et al., 2006).

7.6. Temperature of melting and inferred melt reactions

The temperature regime during partial melting, can be estimated from the saturation temperature of zircon and monazite in melt, obtained from the Zr and LREE concentration relative to major element compositions (Montel, 1993; Watson and Harrison, 1983). The temperature indicated by these chemical thermometers is the temperature at which the accessory minerals last equilibrated with the melt. This could be (i) the temperature at which the magma was extracted from the source, (ii) represent a temperature on the cooling path after melt

Table 4
Estimates of degrees of partial melting using the equation: $F = (C_S - C_0)/C_S$.

	Protolith	Melanosomes							
	Mo10408	Mel-1	F	Mel-2	F	Mel-3	F	Mel-4	F
TiO_2	0.6	0.82	0.27	0.74	0.19	0.73	0.18	0.86	0.30
Fe_2O_3	5.64	6.66	0.15	6.89	0.18	6.28	0.10	6.7	0.16
MgO	2.76	2.72		3.42	0.19	2.85	0.03	2.77	0.01
Zr	160	209	0.23	241	0.34	235	0.32	239	0.33
V	87	102	0.15	114	0.24	108	0.19	109	0.20
Nb	14.5	17.5	0.17	19.7	0.26	19.8	0.27	19.2	0.24
$F_{average}$=			0.19		0.23		0.18		0.21

Major elements are expressed in wt.% and trace elements in ppm.

Table 5
Estimates of degrees of melt extraction in metatexite migmatites using equation: $F = (C_S - C_0) / C_S$.

	Protolith	Metatexites (whole-rock)							
	Mo10408	MO38	F	Res. Mol	F	MO37	F	ResB	F
TiO_2	0.60	0.69	0.14	0.70	0.14	0.79	0.24	0.77	0.22
Fe_2O_3	5.64	6.78	0.17	6.59	0.14	7.24	0.22	7.62	0.26
MgO	2.76	2.98	0.07	2.98	0.08	3.13	0.12	3.50	0.21
Zr	160	174	0.08	214	0.25	214.2	0.25	225	0.29
V	87	109	0.20	105	0.17	124	0.30	114	0.24
Nb	14.5	17	0.14	16.4	0.12	19.1	0.24	19.7	0.26
$F_{average}$=			0.13		0.15		0.23		0.25

Major elements are expressed in wt.% and trace elements in ppm.

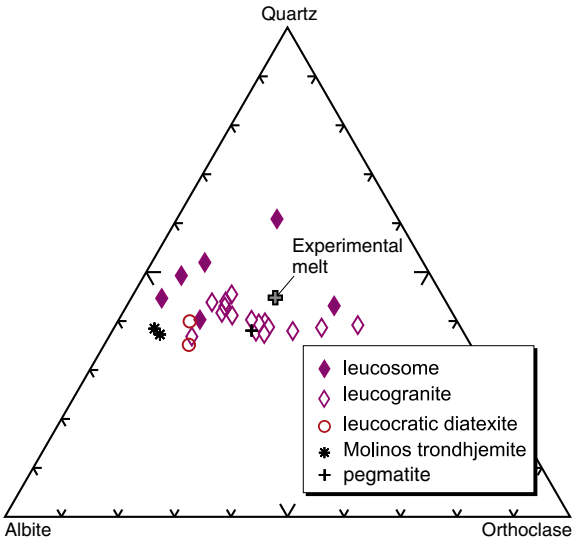

Fig. 13. Albite–quartz–orthoclase normative diagram showing the compositional range of Molinos samples compared to experimentally generated melt from Patiño Douce and Harris (1998) [dehydration melting, starting material = muscovite–biotite schist (MBS), 750 °C and 6 kbar].

had already segregated from its source or (iii) represent the temperature of melting before segregation occurred (see Montel, 1993 and reference therein). Reliable saturation temperatures can be expected only when minor inherited accessory phases exist, otherwise, temperature would be overestimated. Despite this, a tolerance range is allowed e.g. 10% inherited monazite or 10% monazite in the residuum result only in a difference of 10 °C (Montel, 1993). Migmatite leucosomes and leucogranites with (FeOt + MgO) <2 wt.% should provide good

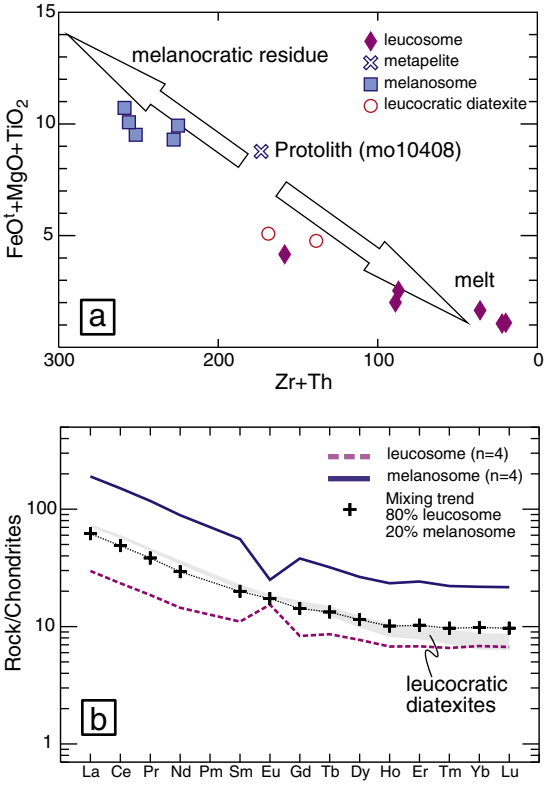

Fig. 15. a) Bivariant diagram of U + Th, representing the relative contents of zircon and monazite and FeOt + MgO + TiO_2, representing the relative contents of biotite. There is a clear correlation between U and Th contents and the proportion of biotite in the rocks. b) Modeled REE pattern showing the effect of adding biotite with accessory phase inclusions. The REE pattern of leucocratic diatexites is reproduced by mixing the leucosome and melanosome fractions.

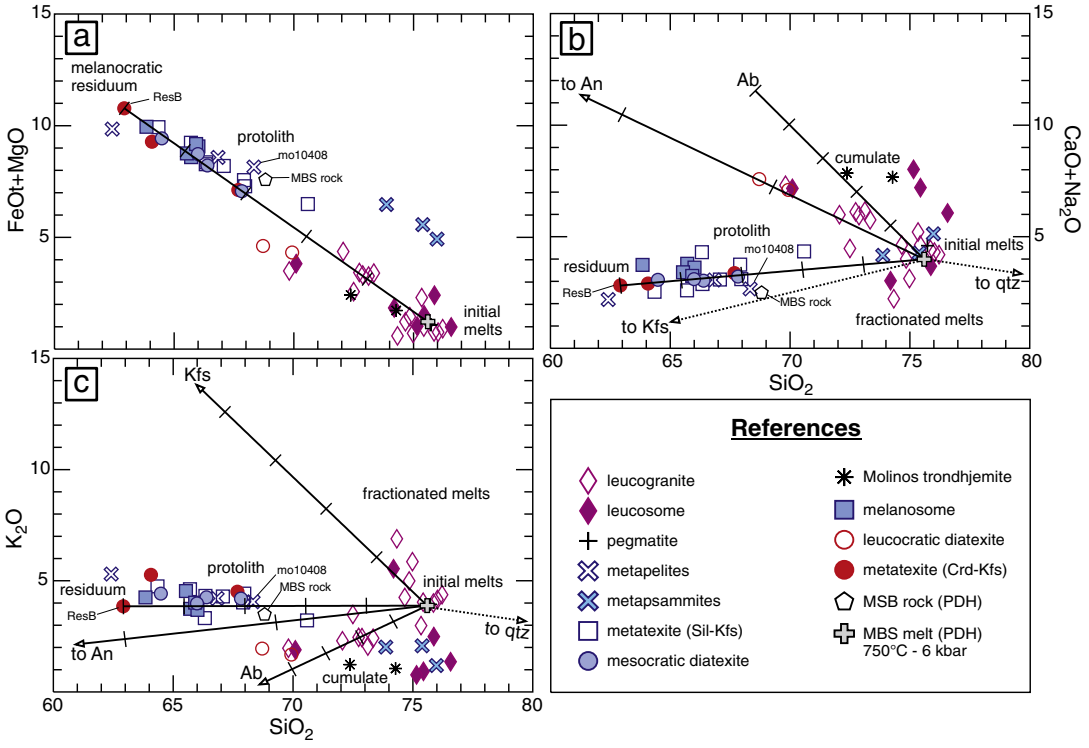

Fig. 14. Harker diagrams in terms of vectors for initial melts, residual compositions and for ideal mineral phases (albite, anothite, orthoclase, and quartz). Recalculated to 100 wt.% anhydrous. MBS rock = muscovite–biotite schist; MBS melt = experimentally generated melt (dehydration-melting, 750 °C and 6 kbar) from Patiño Douce and Harris (1998).

temperature estimates, because these samples are closer to the experimental melt range (Fig. 14a), indicating negligible or minor entrainment of ferromagnesian residual phases containing zircon and monazite as inclusions (see Section 7.4). While inheritance or cumulus of accessory phases would increase the estimated temperatures, the crystal accumulation of main rock-forming minerals would have an opposite effect. However, numerical modeling for zircon saturation thermometry has shown that moderate accumulation of plagioclase or K-feldspar (40–50%) would have little effect on the calculated saturation temperatures for normal granitic compositions (Janoušek, 2006).

The zircon saturation temperatures obtained for residuum-poor leucosomes and leucogranites range from 624 °C to 698 °C with a mean value of 657 °C (Fig. 16a). The monazite saturation temperature varies from 620 °C to 687 °C with a mean of 661 °C (Fig. 16b). There is a visible agreement between these two chemical thermometers (Fig. 16), suggesting that monazite and zircon are fractionated from granitic melts during the same magmatic event. The highest saturation temperature of approximately 700 °C yielded by both thermometers is consistent with muscovite dehydration melting as the principal melt-producing reaction for the inferred pressure of 4–6 kbar. Nonetheless, K-feldspar- and cordierite-bearing neosomes/leucosomes in higher grade migmatites are good indicators that biotite dehydration melting also took place (e.g. Spear et al., 1999). This can be seen more clearly in the petrogenetic grid of Fig. 17, where the peak metamorphic assemblage and the melt production are consistent with a large divariant field suggesting that the first major melting reaction encountered is:

$$\text{Muscovite} + \text{plagioclase} + \text{quartz} \leftrightarrow Al_2SiO_5 + \text{K}-\text{feldspar} + \text{liquid}$$

followed by the continuous reaction:

$$\text{Biotite} + Al_2SiO_5 \leftrightarrow \text{cordierite} + \text{K}-\text{feldspar} + \text{liquid}$$

Dehydration-melting of biotite, however, is probably very limited under the ambient temperatures obtained by saturation thermometry. Furthermore, this is expected because biotite remained stable and occurs in high proportion in residual rocks. Finally, the abundance of late muscovite in some migmatitic rocks require the retrograde P–T path of the Sierra de Molinos to have passed at pressures above IP1 (Fig. 17; 650 °C and 3.8 kbar).

8. Conclusions

The occurrence of all gradations from thin granite streaks to wider veins, sheets and plutons, suggests the formation of the granitoids by anatexis of metasedimentary rocks of the Puncoviscana sequence. The studied suite of rocks represents different elements of an anatectic system active during the Famatinian Orogenic Cycle, under low pressure (4–6 kbar) conditions.

- The U–Pb system in zircons from granitoids and migmatites provided identical ages within analytical errors and indicate that the metamorphic peak and anatectic granite generation occurred at ca. 470 Ma.
- Petrological and compositional data suggest that migmatites of this region are the result of open system processes and that fluid-absent melting played a major role in the formation of migmatites and leucogranites. The association between the HT–LP metamorphic complex, migmatites and leucogranites is interpreted as a melt drainage system for melt migration during deformation-enhanced melt extraction processes in the middle to upper crust.
- The main processes identified in the evolution and diversification of the anatectic magmas are: 1) the varying degree of separation between initial melt and residue. This process would be dominant during the stage of partial melting with increasing temperature, and 2) fractional crystallization during the cooling step, resulting in felsic cumulates and evolved magmas.
- The distribution of inherited zircons ages is virtually identical in the high grade diatexites as in the Puncoviscana Formation. This coincidence, allows on one hand the formation Puncoviscana to be identified among other possible metasedimentary sources and secondly gives validity to the restite-unmixing model at least at the initial stages of the partial melting.

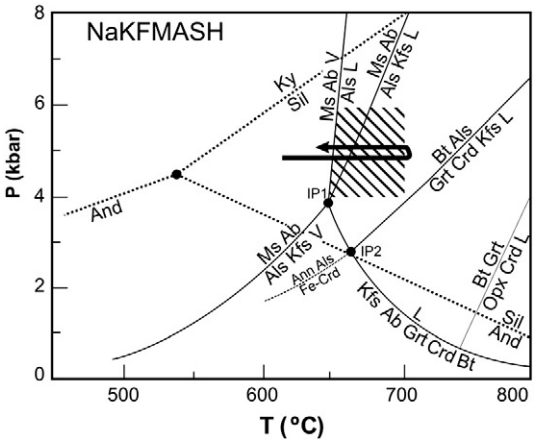

Fig. 17. Simplified petrogenetic grid for pelitic rocks in the Na_2O–K_2O–FeO–MgO–Al_2O_3–SiO_2–H_2O system (Spear et al., 1999) showing the principal melt reactions and the estimated conditions for migmatization and granite formation (hatched area). The black arrow shows the inferred P–T path.

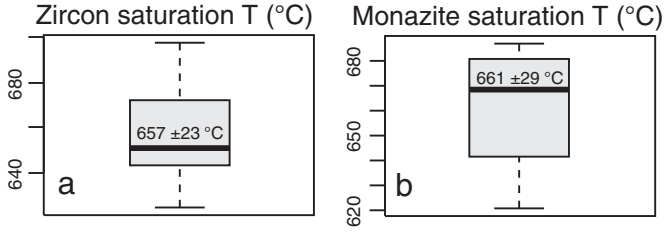

Fig. 16. Zircon and monazite saturation temperature calculations for residuum-poor leucosomes and leucogranites from Sierra de Molinos a) Boxplot showing calculated zircon saturation temperature (Watson and Harrison, 1983) for metatexite leucosomes and leucogranites. b) Boxplot showing calculated monazite saturation temperature (Montel, 1993) for metatexite leucosomes and leucogranites. The boxes in a) and b) represent 50% of the population; the horizontal line inside it is the median; the whiskers delimit the total range.

Acknowledgments

The authors gratefully acknowledge J. Otamendi and the anonymous reviewer for helpful comments and constructive suggestions. J. Otamendi and F. Farina are also thanked for fruitful discussion and critical revision of an earlier version of the manuscript. Marco Scambelluri is thanked for the editorial work. This publication is derived from part of the Ph.D. dissertation of A. Sola, funded by the *Consejo Nacional de Investigaciones Científicas y Técnicas* (CONICET), at the *Universidad Nacional de Salta, Argentina*. We wish to thank those who have helped us in the field work in particular: R. Chocobar, N. Suzaño, R. Salas, F. Hongn. We thank M. Matteini, B. Lima (University of Brasilia), R. Pereyra and A. Nievas (University of Salta), for their assistance in chemical and isotopic analyses. Financial support for field and laboratory

work was provided by projects: PIP 6103 CONICET; 1350/1 and 1790/1 CIUNSa-UNSa.

Appendix A

Analytical procedures

Whole-rock chemistry

Whole-rock samples were pulverized in a Herzog mill into a tungsten carbide shatter-box, then put in a drying chamber at 105 °C for 24 h. Samples were analyzed by X-ray fluorescence spectroscopy (XRF) at the Universidad de Salta Laboratories with a Rigaku 2000 and calibrated against international standards of the appropriate compositions. Major oxides were determined on fusion pellets, and Rb, Sr, Ba, Zr, Nb, Y, and V analyses were performed on pressed powders. A subset of samples was also analyzed for refractory and REE by ICP mass spectrometry method at Acme Analytical Laboratories Ltd. and ALS Laboratory Group (samples Leu1-2–3–4, Mel1-2–3–4, MelGral, Dtxleu1 and Dtxleu2), following a Lithium metaborate/tetraborate fusion and nitric acid digestion.

Geochronology (LA-ICP-MS)

Zircon concentrates were extracted from approximately 4–10 kg rock samples using conventional gravimetric and magnetic (Frantz isodynamic separator) techniques at the Universidad de Salta Laboratories, Argentina. Final purification was achieved by hand picking using a binocular microscope at the University of Brasilia Geochronology Laboratory. Analyses of in situ U–Pb geochronology were performed at the University of Brasília using Neptune ICP-MS multicollector equipment with a UP213 New Wave™ laser ablation probe. For in situ analysis, zircon grains were placed on epoxy® resin mounts, polished and cleaned with 3% nitric acid before analysis. Selection of grains was made avoiding inclusions and fractures. Conditions of laser at time of measure were: 9 Hz frequency, 30 μm spot size, and 39–45% energy. The U–Pb analyses on zircon grains were carried out using the standard-sample bracketing method (Albarède et al., 2004) using the GJ-1 standard zircon in order to control the ICP-MS fractionation. Two to four samples have been analyzed between GJ-1 standard analyses and $^{206}Pb/^{207}Pb$ and $^{206}Pb/^{238}U$ ratios have been time corrected. When necessary to correct the laser induced fractionation the $^{206}Pb/^{238}U$ ratio was recalculated using the linear regression method (Košler et al., 2002). The raw data processed off-line and reduced using an Excel worksheet (Buhn et al., 2009). During analytical session zircon standard UQ-Z1 (Machado and Gauthier, 1996) has been analyzed as an unknown sample (1146 ± 47 Ma = $^{207}Pb/^{206}Pb$ mean age measured). Analyses in some samples were guided by backscattered images carried out at the Federal Police Department in Brasília.

Isotopic Sr–Nd data

Sm–Nd and Rb–Sr isotopic analyses followed the method described by Gioia and Pimentel (2000) and were carried out at the Geochronology Laboratory of the University of Brasília. Whole-rock powders (~70 mg) were mixed with a ^{149}Sm–^{150}Nd spike solution and dissolved in Savillex® capsules. Sm and Nd extraction and purification followed conventional cation exchange techniques, with Teflon columns containing LN-Spec resin (HDEHP–diethylhexyl phosphoric acid supported by PTFE powder). Sm and Nd samples were loaded on Re evaporation filaments of double filament assemblies, and the isotopic measurements were carried out using a multicollector Finnigan MAT 262 mass spectrometer operated in static mode. Two sigma uncertainties in $^{147}Sm/^{144}Nd$ and $^{143}Nd/^{144}Nd$ ratios are better than 0.1% and 0.005%, respectively, according to repeated analyses of international rock standards BHVO-1 and BCR-1. $^{143}Nd/^{144}Nd$ ratios were normalized to $^{146}Nd/^{144}Nd$ 0.7219, and the decay constant used was 6.54×10^{-12} a^{-1}.

References

Aceñolaza, F.G., Miller, H., Toselli, A.J., 1988. The Puncoviscana Formation (Late Precambrian–Early Cambrian)—sedimentology, tectonometamorphic history and age of the oldest rocks of NW Argentina. In: Bahlburg, H., Breitkreuz, Ch., Giese, P. (Eds.), The Southern Central Andes, Contributions to Structure and Evolution of an Active Continental Margin. Lecture Notes in Earth Sciences. Springer, pp. 25–37.

Aceñolaza, F.G., Miller, H., Toselli, A.J., 2000. The Pampean and Famatinian cycles—superposed orogenic events in West Gondwana. In: Miller, H., Hervé, F. (Eds.), Geoscientific Cooperation with Latin America. Zeitschrift für Angewandte Geologie, Sonderheft SH1., 31st International Geological Congress, pp. 337–344.

Adams, C.J., Miller, H., Toselli, A.J., Griffin, W.L., 2008. The Puncoviscana Formation of Northwest Argentina. U–Pb geochronology of detrital zircons and Rb–Sr metamorphic ages and their bearing on its stratigraphic age, sediment provenance and tectonic setting. Neues Jahrbuch für Paläontologie 247 (3), 341–352.

Ague, J.J., 1994. Mass transfer during barrovian metamorphism of pelites, south-central Connecticut, I: evidence for composition and volume change. American Journal of Science 294, 989–1057.

Albarède, F., Telouk, P., Blichert-Toft, J., Boyet, M., Agranier, A., Nelson, B., 2004. Precise and accurate isotopic measurements using multiple-collector ICPMS. Geochimica et Cosmochimica Acta 68 (12), 2725–2744.

Bahlburg, H., Hervé, F., 1997. Geodynamic evolution and tectonostratigraphic terranes of northwestern Argentina and northern Chile. Geological Society of American Bulletin 109, 869–884.

Barker, F., 1979. Trondhjemite: definition, environment and hypotheses of origin. In: Barker, F. (Ed.), Trondhjemites, Dacites, and Related Rocks. Developments in Petrology 6. Elsevier, Amsterdam, pp. 1–12.

Bea, F., 1996. Residence of REE, Y, Th and U in granites and crustal protoliths: implications for the chemistry of crustal melts. Journal of Petrology 37, 521–552.

Becchio, R., Luccassen, F., Franz, G., Viramonte, J., Wemmer, K., 1999. El Basamento Paleozoico Inferior del noroeste de Argentina (23°–27°). Metamorfismo y geocronología. Relatorio del XIV Congreso Geológico Argentino, Salta, vol. 1, pp. 58–78.

Brown, M., 1973. The definition of metatexis, diatexis and migmatite. Proceedings of the Geologists' Association 84, 371–382.

Brown, M., 2001. Orogeny, migmatites and leucogranites: a review. Proceedings of the Indian National Science Academy 110, 313–336.

Buhn, B., Pimentel, M.M., Matteini, M., Dantas, E., 2009. High spatial resolution analysis of Pb and U isotopes for geochronology by laser ablation multi-collector inductively coupled plasma mass spectrometry (LA-MC-ICP-MS). Annals of the Brazilian Academy of Sciences 81, 99–114.

Büttner, S., Glodny, J., Lucassen, F., Wemmer, K., Erdtmann, S., Handler, R., Franz, G., 2005. Ordovician metamorphism and plutonism in the Sierra de Quilmes metamorohic complex: implications for the settings of the nothern Sierras Pampeanas (NW Argentina). Lithos 83, 143–181.

Clemens, J.D., Droop, G.T.R., 1998. Fluids, P–T paths and the fates of anatectic melts in the Earth's crust. Lithos. http://dx.doi.org/10.1016/S0024-4937(98)00020-6.

DoCampo, M., Guevara, S.R., 2005. Provenance analysis and tectonic setting of late Neoproterozoic metasedimentary successions in NW Argentina. Journal of South American Earth Sciences 19, 143–153.

Dominguez, F., Becchio, R., Viramonte, J.G., Martino, R., Pimentel, M., 2006. El basamento ígneo-metamórfico del borde occidental del salar Centenario. Petrografía y estructura. Puna Austral. Salta. Avances en microtectónica y geología estructural. Revista de la Asociación Geológica Argentina, Serie D 9, 161–168.

Ducea, M.N., Otamendi, J.E., Bergantz, G., Stair, K.M., Valencia, V.A., Gehrels, G.E., 2010. Timing constraints on building an intermediate plutonic arc crustal section: U–Pb zircon geochronology of the Sierra Valle Fértil–La Huerta, Famatinian arc, Argentina. Tectonics 29, TC4002. http://dx.doi.org/10.1029/2009TC002615.

Fernandez, C., Becchio, R., Castro, A., Viramonte, J.M., Moreno-Ventas, I., Corretgé, J.G., 2008. Massive generation of atypical ferrosilicic magmas along the Gondwana active margin: implications for cold plumes and back-arc magma generation. Gondwana Research 14, 451–473.

Franz, G., Lucassen, F., Kramer, W., Trumbull, R.B., Romer, R.L., Wilke, H.G., Viramonte, J.G., Becchio, R., Siebel, W., 2006. Crustal evolution at the Central Andean continental margin: a geochemical record of crustal growth, recycling and destruction. In: Oncken, O., Chong, G., Franz, G., Giese, P., Götze, H.-J., Ramos, V.A., Strecker, M.R., Wigger, P. (Eds.), The Andes: Active Subduction Orogeny. Frontiers in Earth Sciences 1. Springer, Heidelberg, pp. 45–64.

Galliski, M.A., Miller, C., 1989. Petrogénesis de las trondhjemitas de Cachi: condicionamientos impuestos por elementos de Tierras Raras e Implicancias Tectónicas. Actas Reunión Geotransectas de América del Sur, pp. 58–62.

Galliski, M.A., Toselli, A.J., Saavedra, J., 1990. Petrology and geochemistry of the Cachi high-alumina trondhjemites, northwestern Argentina. In: Kay, S.M., y Rapela, C.W. (Eds.), Plutonism from Antartica to Alaska. Geological Society of America, Special Paper, 241, pp. 91–99.

García, H.H., Rossello, E.A., 1984. Geología y yacimientos minerales de Papachacra, Depto. Belén, Catamarca, Argentina. Actas, IX Congreso Geológico Argentino, San Carlos de Bariloche, 7, pp. 245–259.

Gioia, S.M.C., Pimentel, M., 2000. The Sm–Nd isotopic method in the Geochronology Laboratory of University of Brasilia. Anais da Academia Brasileira de Ciências 72, 219–245.

Haschke, M., Deeken, A., Insel, N., Sobel, E., Grove, M., Schmitt, A., 2005. Growth pattern of the Andean Puna plateau constrained by apatite (U/Th)/He, K-feldspar 40Ar/39Ar, and zircon U–Pb geochronology. Proceedings, 6th International Symposium on Andean Geodynamics (ISAG 2005, Barcelona), pp. 360–363.

Hongn, F., Becchio, R., 1999. Las fajas miloníticas de Brealito, basamento de los Valles Calchaquíes, Provincia de Salta. Revista de la Asociación Geológica Argentina 54/1, 74–87.

Hongn, F.D., Mon, R., 1999. La deformación ordovícica en el borde oriental de la Puna. In: González Bonorino, G., Omarini, R., Viramonte, J.G. (Eds.), Geología del Noroeste Argentino. Relatorio 148 Congreso Geológico Argentino, vol. 1, pp. 212–216.
Hongn, F.D., Mon, R., Cuevas, J., Tubía, J.M., 1996. Esquisse structural et cinématique de zones de cisaillement calédoniennes à haute température dans la Quebrada Barranquilla, Puna Orientale (Argentina). Comptes Rendus de l'Académie des Sciences 323, 809–815.
Janoušek, V., 2006. Saturnin, R language script for application of accessory-mineral saturation models in igneous geochemistry. Geologica Carpathica 57 (2), 131–142.
Jêzek, P., 1990. Análisis sedimentológico de la Formación Puncoviscana entre Tucumán y Salta. In: Aceñolaza, F., Miller, H., Toselli, A.J. (Eds.), El Ciclo Pampeano en el noroeste argentino. Serie Correlación Geológica. Tucumán, 4, pp. 9–36.
Košler, J., Fonneland, H., Sylvester, P., Tubrett, M., Pedersen, R.B., 2002. U–Pb dating of detrital zircons for sediment provenance studies—a comparison of laser ablation ICP-MS and SIMS techniques. Chemical Geology 182, 605–618.
Lork, A., Bahlburg, H., 1993. Precise U–Pb ages of monazites from the faja eruptiva de la Puna oriental, and the Cordillera Oriental, NW Argentina. Actas XII Congreso Geológico Argentino Congreso Exploración de Hidrocarburos 4, 1–6.
Lork, A., Miller, H., Kramm, U., 1989. U–Pb zircon and monazite ages of la Angostura granite and the orogenic history of the northwestern Argentine basement. Journal of South American Earth Sciences 2, 147–153.
Lork, A., Grauert, B., Kramm, U., Miller, H., 1991. U–Pb investigations of monazite and polyphase zircon: implications for age and petrogenesis of trondhjemites of the southern Cordillera Oriental, NW Argentina. Actas, 6th Congreso Geológico Chileno (Viña del Mar). Servicio Nacional de Geología y Minería, Santiago de Chile, pp. 398–402.
Lucassen, F., Becchio, R., 2003. Timing of high-grade metamorphism: early Palaeozoic U–Pb formation ages of titanite indicate long-standing high-T conditions at the western margin of Gondwana (Argentina, 26–29ºS). Journal of Metamorphic Geology 21, 649–664.
Lucassen, F., Becchio, R., Wilke, H.G., Franz, G., Thirlwal, M.F., Viramonte, J.G., Wemmer, K., 2000. The Paleozoic Basement of the Central Andes (18°–26°S)—a metamorphic view. Journal of South American Earth Sciences 13, 697–715.
Lucassen, F., Becchio, R., Harmon, R., Kasemann, S., Franz, G., Trumbull, R., Wilke, H.-G., Romer, R.L., Dulski, P., 2001. Composition and density model of the continental crust in an active continental margin—the Central Andes between 18° and 27°S. Tectonophysics 341, 195–223.
Lucassen, F., Becchio, R., Franz, G., 2011. The Early Palaeozoic high-grade metamorphism at the active continental margin of West Gondwana in the Andes (NW Argentina/N Chile). International Journal of Earth Sciences 100, 445–463.
Machado, N., Gauthier, G., 1996. Determination of $^{206}Pb/^{207}Pb$ ages on zircon and monazite by laser ablation ICPMS and application to a study of sedimentary provenance and metamorphism in southeastern Brazil. Geochimica et Cosmochimica Acta 60, 5063–5073.
Méndez, V., Nullo, F., Otamendi, J., 2006. Geoquímica de las Formaciones Puncoviscana y Cachi-Sierra de Cachi, Salta. Revista de la Asociación Geológica Argentina 61, 256–268.
Milord, I., Sawyer, E.W., Brown, M., 2001. Formation of diatexite migmatite and granite magma during anatexis of semi-pelitic metasedimentary rocks: an example from St. Malo, France. Journal of Petrology 42, 487–505.
Montel, J.M., 1993. A model for monazite/melt equilibrium and application to the generation of granitic magmas. Chemical Geology 110, 127–146.
Omarini, R.H., Sureda, R.J., Götze, H.-J., Seilacher, A., Pflüger, F., 1999. Puncoviscana folded belt in northwestern Argentina: testimony of Late Proterozoic Rodinia fragmentation and pre-Gondwana collisional episodes. International Journal of Earth Sciences 88, 76–97.
Pankhurst, R.J., Rapela, C.W., Fanning, C.M., 2000. Age and origin of coeval TTG, I- and S-type granites in the Famatinian belt of NW Argentina. Transactions of the Royal Society of Edinburgh: Earth Science 91, 151–168.
Patiño Douce, A.E., Harris, N., 1998. Experimental constraints on Himalayan anatexis. Journal of Petrology 39 (4), 689–710.
Prinzhofer, A., Allegre, C.J., 1985. Residual peridotites and the mechanisms of partial melting. Earth and Planetary Science Letters 74, 251–265.
Ramos, V., 1999. Rasgos estructurales del territorio argentino. Evolución tectónica de la Argentina. In: Caminos, R. (Ed.), Geología Argentina. Instituto de Geología y Recursos Minerales, Anales, 29, pp. 715–784.
Ramos, V., 2008. The basement of the Central Andes: the Arequipa and Related Terranes. Annual Review of Earth and Planetary Sciences 36, 289–324.
Rapela, C.W., Toselli, A., Kearnan, L., Saavedra, J., 1990. Granite plutonism of the Sierras Pampeanas: an inner cordilleran Paleozoic arc in the southern Andes. In: Kay, S.M., Rapela, C.W. (Eds.), Plutonism from Antarctica to Alaska. Geological Society of America Special Papers, 241, pp. 77–90.
Rossi, J.N., Toselli, A.J., Durand, F.R., 1992. Metamorfismo de baja presión, su relación con el desarrollo de la cuenca Puncoviscana, plutonismo y régimen tectónico. Argentina. Estudios Geológicos. http://dx.doi.org/10.3989/egeol.92485-6394.
Sawyer, E.W., 1991. Disequilibrium melting and the rate of melt–residuum separation during migmatization of mafic rocks from the Grenville Front, Quebec. Journal of Petrology 32, 701–738.
Sawyer, E.W., 1998. Formation and evolution of granite magmas during crustal reworking: the significance of diatexites. Journal of Petrology 39, 1147–1167.
Sawyer, E.W., 1999. Criteria for the recognition of partial melting. Physics and Chemistry of the Earth, Part A: Solid Earth and Geodesy 24, 269–279.
Sawyer, E.W., 2008. Atlas of migmatites. The Canadian Mineralogist, Special Publication 9.NRC Research Press, Ottawa, Ontario, Canada (371 pp.).
Sola, A.M., Becchio, R.A., Pimentel, M.M., 2010. Leucogranito Pumayaco: anatexis cortical durante el Ciclo Orogénico Famatiniano en el Extremo Norte de la Sierra De Molinos, Provincia de Salta. Revista de la Asociación Geológica Argentina 66 (1), 206–224.
Solar, G., Brown, M., 2001. Petrogenesis of migmatites in Maine, USA: possible source of peraluminous leucogranite in plutons? Journal of Petrology 42 (4), 789–823.
Spear, F.S., Kohn, M.J., Cheney, J.T., 1999. P–T paths from anatectic pelites. Contributions to Mineralogy and Petrology 134, 17–32.
Stevens, G., Clemens, J.D., 1993. Fluid-absent melting and the roles of fluids in the lithosphere: a slanted summary? Chemical Geology. http://dx.doi.org/10.1016/0009-2541(93)90314-9.
Sun, S., McDonough, W.F., 1989. Chemical and isotopic systematics of oceanic basalts: implications for mantle composition and processes. In: Saunders, A.D., Norry, M.J. (Eds.), Magmatism in the Ocean Basins. Geological Society Special Publication, vol. 42, pp. 313–345. http://dx.doi.org/10.1144/GSL.SP.1989.042.01.19.
Taylor, S.R., McLennan, S.M., 1985. The Continental Crust: its Composition and Evolution. Blackwell, Oxford (312 pp.).
Thompson, R.N., 1982. Magmatism of the British Tertiary Volcanic Province. Scottish Journal of Geology 18, 49–107.
Toselli, A.J., Sial, A.J., Rossi, J.N., 2002. Ordovician magmatism of the Sierras Pampeanas, Sistema de Famatina and Cordillera Oriental, NW of Argentina. In: Aceñolaza, F.G. (Ed.), Aspects of the Ordovician System in Argentina, INSUGEO, Serie Correlación Geológica. Tucumán, vol. 16, pp. 313–326.
Vanderhaeghe, O., 2009. Migmatites, granites and orogeny: flow modes of partially-molten rocks and magmas associated with melt/solid segregation in orogenic belts. Tectonophysics 477, 119–134.
Vigneresse, J.L., Barbey, P., Cuney, M., 1996. Rheological transitions during partial melting and crystallization with application to felsic magma segregation and transfer. Journal of Petrology 37, 1579–1600.
Viramonte, J.M., Becchio, R., Viramonte, J.G., Pimentel, M.M., Martino, R.D., 2007. Ordovician igneous and metamorphic units in southeastern Puna: new U–Pb and Sm–Nd data and implications for the evolution of northwestern Argentina. Journal of South American Earth Sciences 24, 167–183.
Watson, E.B., Harrison, T.M., 1983. Zircon saturation revisited: temperature and composition effects in a variety of crustal magma types. Earth and Planetary Science Letters 64, 295–304.
Wegmann, M.I., Riller, U., Hongn, F.D., Glodny, J., Oncken, O., 2008. Age and kinematics of ductile deformation in the Cerro Durazno area, NW Argentina: significance for orogenic processes operating at the western margin of Gondwana during Ordovician–Silurian times. Journal of South American Earth Sciences 26, 78–90.
Wickham, S.M., 1987. The segregation and emplacement of granitic magmas. Journal of the Geological Society of London 144, 281–297.
Yardley, B.W.D., 1989. An Introduction to Metamorphic Petrology. Longman Herat Science Series. (248 pp., London).